ISSN 1063-780X, Plasma Physics Reports, 2012, Vol. 38, No. 5, pp. 407–431. © Pleiades Publishing, Ltd., 2012.
Original Russian Text © A.N. Trushkin, I.V. Kochetov, 2012, published in Fizika Plazmy, 2012, Vol. 38, No. 5, pp. 447–472.

LOW-TEMPERATURE PLASMA

Simulation of Toluene Decomposition in a Pulse-Periodic Discharge Operating in a Mixture of Molecular Nitrogen and Oxygen

A. N. Trushkin and I. V. Kochetov

Troitsk Institute for Innovation and Fusion Research (TRINITI), ul. Pushkovykh 12, Troitsk, Moscow oblast, 142090 Russia

Received July 20, 2011; in final form, October 17, 2011

Abstract—The kinetic model of toluene decomposition in nonequilibrium low-temperature plasma generated by a pulse-periodic discharge operating in a mixture of nitrogen and oxygen is developed. The results of numerical simulation of plasma-chemical conversion of toluene are presented; the main processes responsible for $C_6H_5CH_3$ decomposition are identified; the contribution of each process to total removal of toluene is determined; and the intermediate and final products of $C_6H_5CH_3$ decomposition are identified. It was shown that toluene in pure nitrogen is mostly decomposed in its reactions with metastable $N_2(A^3\Sigma_u^+)$ and $N_2(a'^1\Sigma_u^-)$ molecules. In the presence of oxygen, in the $N_2 : O_2$ gas mixture, the largest contribution to $C_6H_5CH_3$ removal is made by the hydroxyl radical OH which is generated in this mixture exclusively due to plasma-chemical reactions between toluene and oxygen decomposition products. Numerical simulation showed the existence of an optimum oxygen concentration in the mixture, at which toluene removal is maximum at a fixed energy deposition.

DOI: 10.1134/S1063780X12040083

1. INTRODUCTION

Toluene ($C_6H_5CH_3$) is among organic solvents most commonly used in modern chemical, light, textile, numerous paint and varnish industries, and others. Toluene vapor emission into an air medium of industrial facilities and through ventilation exhausts into the atmosphere has an adverse effect on human health and environmental conditions. The characteristic feature of these ventilation flows consists in a comparatively low concentration of toluene vapor, which, nevertheless, exceeds the maximum allowable sanitary norms by several orders of magnitude. In this case, the use of conventional methods of gas purification (thermal burning, catalytic oxidation, absorption, and adsorption methods) becomes inefficient and economically unprofitable. This situation stimulates the search for new more advanced methods for neutralizing gas exhausts. Currently, active studies on the development of nonequilibrium plasma methods of gas purification are performed in all developed countries. These methods are based on the formation of a high concentration of chemically active and ecologically safe particles in polluted gas using nonequilibrium low-temperature plasma without appreciable heating of a treated gas flow. Generated chemically active particles react with pollutant molecules and decompose harmful impurities. In this case, toluene vapor is a very popular object of laboratory studies, used to test the efficiency of nonequilibrium plasma-chemical purification of air from harmful impurities, since toluene vapor is also a very complicated object from the viewpoint of its decomposition and removal from exhaust gas flows [1–6].

The spectrum of the active particles providing the plasma-chemical conversion of toluene is controlled to a large extent by the composition of the treated gas mixture. One of the main components of the most polluted gas flows is molecular nitrogen, in which a significant fraction of the energy deposited into the discharge is stored. Therefore, in recent years, the problem of the role of excited nitrogen molecules and atoms in mechanisms of toluene decomposition in various hydrocarbons is actively discussed. In [7], based on an analysis of the composition of by-products of plasma-chemical decomposition of cyclohexane $C_6H_{10}O$ in the spark discharge, it was assumed that excited metastable nitrogen molecules in the $N_2(A^3\Sigma_u^+)$ state are involved in $C_6H_{10}O$ aromatic ring decomposition. The results of numerical simulation [8] of polyaromatic hydrocarbon $C_{10}H_8$ (naphthalene) removal in nitrogen using the pulsed corona showed that the basic mechanism of naphthalene decomposition is associated with its interaction with excited $N_2(A^3\Sigma_u^+)$ molecules and $N(^2D)$ atoms. Detailed experimental studies of toluene removal in pure nitrogen and its mixtures with oxygen in the dielectric barrier discharge are described in [9]. To explain the results obtained, the authors of [9] propose various channels of the interaction of the toluene molecule with the

metastable $N_2(A^3\Sigma_u^+)$ nitrogen molecule. We note that the purely energy approach to the reaction probability is used in [7–9]: the internal energy content of the $N_2(A^3\Sigma_u^+)$ molecule is sufficient for chemical bond breaking in the hydrocarbon molecule. Such an approach is unobjectionable if particular final reaction products [8] are not indicated. If the final reaction products are indicated [7, 9], to estimate the probability of this reaction, other conservation laws should be considered, in particular, the spin conservation law.

Molecular oxygen, along with nitrogen, exists in various concentrations in polluted gas flows. The oxygen appearance in the initial gas mixture results in generation of new (in comparison with nitrogen) chemically active particles: oxygen atoms O, excited molecules O_2, ozone, and hydroxyl radical OH (due to plasma-chemical reactions), which, at first sight, should significantly increase the efficiency of pollutant removal. However, experimental studies do not give such an unambiguous answer. For example, it was found [10] that a small (≤2%) oxygen additive to nitrogen substantially increases toluene removal in the dielectric barrier discharge (BD); however, an increase in the O_2 concentration in the mixture over 2% results in a decreased efficiency of $C_6H_5CH_3$ removal. Similar results were obtained in [9]. Falkenstein [10] attributes the nonmonotonic behavior of the efficiency of toluene removal to the ozone formation process, in which the oxygen atom, highly active in relation to toluene, is converted into ozone having an extremely low reactivity with $C_6H_5CH_3$. The other point of view to the existence of the optimum oxygen concentration in the mixture $N_2 : O_2$ was advanced in [11]: oxygen is an electronegative gas; therefore, its additives at high concentrations lead to an appreciable decrease in the electron density and the electrical energy contributed to the discharge; at low O_2 concentrations, the effect of electron attachment is insignificant, and generation of highly reactive O atoms comes to the fore. The effect of oxygen additives on the toluene removal efficiency in the glow discharge and spark was studied in [12]. It was found that the amount of removed toluene, as in [10], nonmonotonically depends on the oxygen concentration; however, the reduced efficiency (the amount of removed toluene per unit energy deposited into the discharge) monotonically increases with the O_2 concentration in the mixture. It should be noted that it is rather difficult to make unambiguous conclusions about the effect of oxygen on the toluene removal efficiency based on the experimental results [12], since their interpretation should consider thermal decomposition of toluene in addition to plasma-chemical decomposition: the neutral gas temperature in used discharge types was in the range of 1000–2000 K; in this case, the oxygen content had a significant effect on the gas temperature.

The contribution of direct electron impact dissociation to the process of aromatic hydrocarbon removal was discussed in [11, 13]. The cross sections of electron impact dissociation of aromatic hydrocarbons are currently unknown; therefore, the estimate of the role of this channel in the hydrocarbon removal mechanism is presumable. In [13], to estimate the dependence of the hydrocarbon dissociation rate on the electron temperature, it is proposed to use approximations similar to the Arrhenius law in which the role of the gas temperature is played by the electron temperature. In our opinion, the dissociation rate constant taken in [11] is significantly overestimated for the dielectric barrier discharge conditions, and the conclusion on the crucial role of electron impact dissociation in the xylene removal mechanism seems doubtful.

The above review shows that, despite the large number of experimental studies on toluene decomposition, the concepts on the kinetics of this process are currently in the development stage. A comprehensive kinetic model of plasma-chemical transformations of toluene, which would allow description of the actual kinetics of this process under conditions of nonequilibrium low-temperature plasma of the gas discharge, separation of controlling reactions, and determination of optimum conditions of the process, has not yet been presented in the literature. The available models describe, as a rule, only the first initial stage phase of toluene decomposition, omitting the long chain of intermediate reactions accompanying $C_6H_5CH_3$ plasma decomposition; in this case, comparison with the experiment is performed only by the degree of toluene removal. The absence of the comprehensive model with predictive power significantly complicates critical analysis of available experimental results on plasma-chemical decomposition of toluene, which are obtained under different conditions and often significantly contradict each other. Furthermore, the development of such a model is extremely important from the viewpoint of analysis of intermediate products of $C_6H_5CH_3$ conversion, since modern trends in the development of plasma-chemical gas purification methods consist in the combination of the plasma reactor with a catalyst or an adsorbent [14, 15], which will make it possible to lower significantly the purification energy cost and to achieve total hydrocarbon oxidation to CO_2 and H_2O. As experiments show, such a combination will make it possible to lower significantly the catalyst operating temperature (to room temperature), to increase its efficiency, and to increase absorbing power and capacity of adsorbent. It seems quite reasonable to explain the above effects based on the interaction of the catalyst and adsorbent with active intermediate components produced during decomposition of initial pollutant material.

The main objective of this study is to develop the mathematical model of plasma-chemical processes of

toluene decomposition, initiated by nonequilibrium low-temperature plasma in the mixture of nitrogen and oxygen, to determine basic mechanisms of $C_6H_5CH_3$ removal, to identify the main intermediate and final products of its conversion, and to determine optimum conditions of the process of gas purification from toluene impurities.

2. MODEL

The developed model consists of two interconnected parts: the gas-discharge stage describing the process of nonequilibrium low-temperature plasma generation, the production of chemically active particles and plasma-chemical processes in an external applied electric field, and the postdischarge stage in which plasma-chemical processes occur in the absence of an electric field. The gas-discharge stage is modeled by a periodic sequence of voltage pulses whose pulse-repetition time significantly exceeds the pulse duration. The gas discharge in molecular gases at atmospheric pressure most often is a plasma structure (streamer, spark) sharply inhomogeneous in space and nonstationary in time. In this case, the comprehensive self-consistent description of the discharge should be based on the nonstationary three-dimensional model of gas-discharge and plasma-chemical processes in which the discharge formation should be considered simultaneously with plasma-chemical reactions in the discharge channel. In nonequilibrium low-temperature plasma at atmospheric pressure, a large number of reactions occur, whose spectrum depends to a large extent on the initial gas mixture composition. Currently, it seems impossible to exactly describe the plasma-chemical reactor, taking into account both above factors (plasma inhomogeneity and nonstationarity and a large number of plasma-chemical reactions); therefore, various simplifying assumptions are made in the numerical simulation of actual plasma devices. In this study, numerical calculations were performed for the experimental conditions of [9], in which toluene removal using a unipolar pulse-periodic barrier discharge in the gas mixture $N_2 : O_2$ was studied at atmospheric pressure in the coaxial geometry. The choice of the study [9] as a basis for verifying the developed plasma-chemical model was caused by that, in addition to the determination of the degree of toluene decomposition, a large number of intermediate products of its decomposition were measured. In the experiment [9], the repetition rate of unipolar voltage pulses was varied within $f = 0$–200 Hz; in this case, the typical discharge current pulse duration at half the amplitude was 50 ns. The specific energy deposition into gas was varied by varying the current pulse repetition rate at a fixed gas flow and was within $Q = 0$–400 J/L. The oxygen content in the working mixture was varied within 0–10%. The experiments were performed at two initial toluene concentrations, 100 and 400 ppm.

In [9], the spatial discharge structure was not studied experimentally; in the introduction, the authors a priori make the statement about its spatial inhomogeneity. Since in this paper emphasis is made on the development of the detailed kinetic model of plasma-chemical conversion of toluene, while the discharge development and generation of chemically active particles is described within the spatially uniform model, we present a number of reasons in favor of the use of this model. First, we note the recent experimental work [16] in which the spatial structure of the dielectric barrier discharge in air, excited by nanosecond voltage pulses, was studied using high-speed electron-optical cameras. There was found that the spatial structure of this discharge has a diffuse (not channel) shape. As can be seen from the discharge current and voltage oscillograms presented in [9], the main energy deposition into treated gas occurs not at the leading edge of the current pulse, corresponding to the discharge development stage, but at the trailing edge, when the interelectrode gap is filled with plasma. The initial geometrical inhomogeneity in the electric field distribution over the interelectrode gap in the cylindrical electrode system almost completely disappears when this gap is filled with plasma [17]. In this case, the use of the homogeneous discharge model seems quite reasonable.

At the same time, it is well known from the literature [18] that the dielectric barrier discharge in the gas mixture $N_2 : O_2$ at the sinusoidal voltage with a frequency of 50 Hz to 100 kHz passes from the spatially homogeneous phase in pure nitrogen to the multichannel (microdischarge, MD) mode as the oxygen concentration in the mixture exceeds ~450 ppm. Assuming that such a scenario of the discharge evolution is also possible under conditions of [9], let us show that the homogeneous discharge model can be applied to describe generation of chemically active particles in this case as well. The characteristic radius of an individual microdischarge at atmospheric pressure is about 100 μm, the distance between individual MDs completely filling the interelectrode gap is ~1 mm. The results of experimental studies of recent years [19–21] suggest that chemically active particles are mostly generated in streamer-type discharges at the plasma channel decay stage, when the basic energy deposition into gas occurs. Estimations show that the lifetime of free radicals, electron-exited atoms, molecules, and other chemically active particles (except for ozone which has no appreciable effect on the toluene removal process due to the low rate of ozone reactions with toluene and decomposition products, $k = 10^{-18}$–10^{-22} cm^3/(molecule s)) generated in the discharge under chosen experimental conditions does not exceed 100 μs. For this time, active particles generated in the microdischarge channel have no time to appreciably diffuse from the MD channel to ambient gas; hence, all plasma-chemical reactions mostly occur in the microdischarge channel. Thus, the processes of

active particle transport from the MD volume have no significant effect on the dynamics of toluene removal (we note that this conclusion can become invalid in the case where O_3 is an active reagent, e.g., when removing nitrogen oxides). However, such an energy deposition localized in narrow channels leads to generation of increased concentrations of chemically active particles and, in principle, can cause the appearance of nonlinear processes of mutual recombination of produced radicals. The radical recombination is an undesirable phenomenon from the viewpoint of plasma gas purification, since it causes inefficient expenditure of the energy deposited to the discharge and a decrease in the purification energy efficiency. However, estimations using concentrations of O, H, N, OH radicals, and N_2 and O_2 molecules in electronically excited states, measured in the MD channel [19–22], show that the loss of active particles in nonlinear recombination processes at toluene concentrations of 100 and 400 ppm is small in comparison with their loss in reactions with toluene (at least until the $C_6H_5CH_3$ concentration decreases to ~10 ppm). During linear processes of generated particle expenditure, the toluene removal efficiency is controlled only by the number of these particles and is independent of the spatial distribution of their generation regions.

In the simulation of plasma-chemical processes of toluene decomposition, it was accepted that, according to the experiment, for the time of residence in the discharge region, a given gas portion is subjected to a train of current pulses whose number depends on the voltage pulse repetition rate. For the time between current pulses $t > 5$ ms, the activated gas medium of each individual microdischarge has time to uniformly mix with neighboring microdischarges due to diffusion broadening. Thus, to the beginning of the following current pulse, a uniformly treated gas mixture with a changed composition will be in the entire gas-discharge chamber volume. Such a description corresponds to the instantaneous mixing approximation. Then, this mixture is subjected to the following current pulse and so on. In our opinion, the above arguments (generation and expenditure of active particles in the microdischarge plasma channel, the absence of nonlinear processes of their loss, uniform diffusion mixing of the activated microdischarge medium in pauses between current pulses) show the applicability of the homogeneous model to describe generation of chemically active particles in the dielectric barrier discharge.

The spatially homogeneous model for describing the barrier discharge is constructed based on relevant models of nonequilibrium plasma in atmospheric air [23, 24] and includes more than 100 elementary processes involving electrons, positive and negative ions, molecules and atoms in ground and excited states, and radicals. The basic processes included in this model are listed in Table 1. The model considers excitation of rotational, vibrational, and electronic levels, as well as electron-impact ionization and dissociation of N_2, O_2, and H_2O molecules (H_2O molecules appear in this gas mixture due to plasma-chemical reactions). Some of these processes (excitation of rotational and vibrational levels of molecules) have no direct effect on toluene removal (do not enter the $C_6H_5CH_3$ conversion mechanism); however, their consideration is necessary for correct determination of the electron energy distribution function. The self-consistent set of reduced cross sections for N_2 and O_2, given in [24] was used. As in [24], the total cross section of excitation of vibrational levels of N_2, O_2 and H_2O molecules is used in the present study. In describing the excitation kinetics of nitrogen electronic states, three electronic levels are introduced. The first one corresponds to the lower metastable $N_2(A^3\Sigma_u^+)$ level; the second level corresponds to the sum of the metastable $N_2(a'^1\Sigma_u^-)$ level and $N_2(a^1\Pi_g)$ and $N_2(w^1\Delta_u)$ levels; and the third effective level $N_2(E_{sum})$ corresponds to the sum of other electronic levels. According to the model, the first two metastable levels play an important role in the toluene conversion mechanism. For the O_2 molecule, two metastable $O_2(a^1\Delta_g)$ and $O_2(b^1\Sigma_g^+)$ electronic levels are considered. For nitrogen and oxygen atoms, in addition to ground states, excited metastable $N(^2D)$, $N(^2P)$, and $O(^1D)$ states were taken into account.

As was noted in the Introduction, electron-impact dissociation cross sections of the $C_6H_5CH_3$ molecule are currently unknown; therefore, it seems impossible to accurately calculate the contribution of this process to toluene removal. In this study, we perform model calculations of electron-impact toluene dissociation using approximations for the interaction constants of electrons with the C_6H_6 molecule [13]. These calculations showed that the direct contribution of the electron impact to toluene decomposition to the dielectric barrier discharge does not exceed 2%. Charge exchange reactions of N^+, N_2^+, N_4^+, O^+, O_2^+, and O_4^+ ions on $C_6H_5CH_3$ molecules, which result in toluene removal during the discharge stage, are included into the positive ion kinetics. Accurate constants of these reactions are unknown to the authors; according to [37], they varied in numerical calculations within 10^{-9}–5×10^{-9} cm^3/s. It was found that the contribution of this channel to toluene decomposition under the conditions of this study does not exceed 1%. The electron affinity energy of the toluene molecule is negative [38]; therefore, the formation of negative $C_6H_5CH_3$ ions was ignored in this model. The electron loss is controlled by electron–ion recombination (including that with the $C_6H_5CH_3^+$ ion [36]) and attachment (dissociative and three-body) to electronegative oxygen molecules. For the experimental conditions of [9], as in [24], the ion recombination

Table 1. Main processes included in the gas-discharge stage of the model

No.	Process	Rate constant, s^{-1}, cm^3/s, cm^6/s, $T = 323$ K	Reference
1	$N_2 + e \longrightarrow N_2(\mathrm{rot}) + e$	BE*	[25]
2	$N_2 + e \longrightarrow N_2(V_{\mathrm{sum}}) + e$	BE	[25]
3	$N_2 + e \longrightarrow N_2(A^3\Sigma_u^+) + e$	BE	[25]
4	$N_2 + e \longrightarrow N_2(a'^1\Sigma_u^-) + e$	BE	[25]
5	$N_2 + e \longrightarrow N_2(E_{\mathrm{sum}}) + e$	BE	[25]
6	$N_2 + e \longrightarrow N_2^+ + e + e$	BE	[25]
7	$N_2^+ + e \longrightarrow N + N$	BE	[25]
8	$N_2 + e \longrightarrow N + N + e$	BE	[25]
9	$N + e \longrightarrow N(^2D_0) + e$	BE	[26, 27]
10	$N + e \longrightarrow N(^2P_0) + e$	BE	[26, 27]
11	$N(^2D_0) + e \longrightarrow N(^2P_0) + e$	BE	[26, 27]
12	$N + N + M \longrightarrow N_2(A^3\Sigma_u^+) + M$	1.7×10^{-33} ($M = N_2, O_2$)	[28]
13	$N + N + M \longrightarrow N_2(E_{\mathrm{sum}}) + M$	2.4×10^{-33} ($M = N_2, O_2$)	[28]
14	$N_2(A^3\Sigma_u^+) + N_2(A^3\Sigma_u^+) \longrightarrow N_2(E_{\mathrm{sum}}) + N_2$	4.5×10^{-10}	[25]
15	$N_2(E_{\mathrm{sum}}) + N_2 \longrightarrow N_2(A^3\Sigma_u^+) + N_2$	3.0×10^{-11}	[25]
16	$N_2(a'^1\Sigma_u^-) + N_2 \longrightarrow N_2(E_{\mathrm{sum}}) + N_2$	2.0×10^{-13}	[23]
17	$O_2 + e \longrightarrow O_2(\mathrm{rot}) + e$	BE	[29]
18	$O_2 + e \longrightarrow O_2(V_{\mathrm{sum}}) + e$	BE	[29]
19	$O_2 + e \longrightarrow O + O + e$	BE	[29]
20	$O_2 + e \longrightarrow O + O(^1D) + e$	BE	[29]
21	$O_2(V_{\mathrm{sum}}) + e \longrightarrow O + O + e$	BE	[29]
22	$O_2 + e \longrightarrow O_2(a^1\Sigma) + e$	BE	[29]
23	$O_2 + e \longrightarrow O_2(b^1\Sigma) + e$	BE	[29]
24	$O_2(a^1\Delta) + e \longrightarrow O + O + e$	BE	[29]
25	$O_2(b^1\Delta) + e \longrightarrow O + O + e$	BE	[29]
26	$O_2(a^1\Delta) + e \longrightarrow O_2(b^1\Sigma) + e$	BE	[29]
27	$O_2 + e \longrightarrow O^- + O$	BE	[29]
28	$O_2(V_{\mathrm{sum}}) + e \longrightarrow O^- + O$	BE	[29]
29	$O_2(a^1\Delta) + e \longrightarrow O^- + O$	BE	[29]
30	$O_2(b^1\Sigma) + e \longrightarrow O^- + O$	BE	[29]
31	$O_3 + e \longrightarrow O^- + O_2$	BE	[29]
32	$O_2 + e + O_2 \longrightarrow O_2^- + O_2$	BE	[29]
33	$O_2 + e + N_2 \longrightarrow O_2^- + N_2$	BE	[29]
34	$O_2 + e \longrightarrow O_2^+ + e + e$	BE	[29]
35	$O_2(a^1\Delta) + e \longrightarrow O_2^+ + e + e$	BE	[29]

Table 1. (Contd.)

No.	Process	Rate constant, s^{-1}, cm^3/s, cm^6/s, $T = 323$ K	Reference
36	$O_2(b^1\Sigma) + e \longrightarrow O_2^+ + e + e$	BE	[29]
37	$O_2 + e \longrightarrow O^+ + O + e + e$	BE	[29]
38	$O_2^+ + e \longrightarrow O + O$	BE	[29]
39	$O^- + O_2^+ \longrightarrow O + O_2$	3.0×10^{-7}	[24]
40	$O_2^- + O_2^+ \longrightarrow O_2 + O_2$	1.1×10^{-6}	[24]
41	$O_2^- + N_4^+ \longrightarrow N_2 + N_2 + O_2$	1.1×10^{-6}	[24]
42	$O_2^- + O_4^+ \longrightarrow O_2 + O_2 + O + O$	1.1×10^{-6}	[24]
43	$O_2^+ + O_2 + O_2 \longrightarrow O_4^+ + O_2$	2.4×10^{-30}	[24]
44	$O_4^+ + e \longrightarrow O_2 + O_2$	2.2×10^{-7}	[24]
45	$N_4^+ + O_2 \longrightarrow O_2^+ + N_2 + N_2$	2.5×10^{-10}	[23]
46	$O_4^+ + O \longrightarrow O_2^+ + O_3$	3.0×10^{-10}	[24]
47	$O_4^+ + O^- \longrightarrow O_2 + O_3$	1.1×10^{-6}	[24]
48	$H_2O + e \longrightarrow H + OH + e$	BE	[30]
49	$H_2O + e \longrightarrow H^- + OH$	BE	[30]
50	$H_2O + e \longrightarrow H_2 + O^-$	BE	[30]
51	$H_2O + e \longrightarrow H_2O^+ + e + e$	BE	[20]
52	$O + e \longrightarrow O(^1D) + e$	BE	[29]
53	$O_3^- + O^+ \longrightarrow O_2 + O_2$	3.8×10^{-7}	[29]
54	$O_3^- + O_2^+ \longrightarrow O + O + O_3$	1.0×10^{-7}	[29]
55	$O_3^- + O_4^+ \longrightarrow O_2 + O_2 + O_3$	1.1×10^{-6}	[24]
56	$O^- + O_2 \longrightarrow O_3 + e$	5.0×10^{-15}	[29]
57	$O_3^- + O_3 \longrightarrow O_2 + O_2 + O_2 + e$	1.0×10^{-10}	[29]
58	$O_2^- + N \longrightarrow NO_2 + e$	5.5×10^{-10}	[24]
59	$O_2^- + N \longrightarrow NO + O + e$	5.5×10^{-10}	[24]
60	$O^- + N \longrightarrow NO + e$	2.6×10^{-10}	[24]
61	$O^- + CO \longrightarrow CO_2 + e$	5.5×10^{-10}	[31]
62	$H^- + O_2 \longrightarrow HO_2 + e$	1.5×10^{-9}	[31]
63	$OH^- + N \longrightarrow HNO + e$	1.0×10^{-11}	[31]
64	$OH^- + O \longrightarrow HO_2 + e$	2.0×10^{-10}	[31]
65	$OH^- + H \longrightarrow H_2O + e$	1.0×10^{-9}	[24]
66	$N_2(A^3\Sigma_u^+) + O_2 \longrightarrow N_2 + O + O$	4.0×10^{-12}	[24]
67	$N_2(E_{sum}) \longrightarrow N_2(A^3\Sigma_u^+) + h\nu$	2.0×10^5	[24]
68	$N_2(A^3\Sigma_u^+) + O_2 \longrightarrow N_2O + O$	4.6×10^{-15}	[24]
69	$N_2(a'^1\Sigma_u^-) + O_2 \longrightarrow N_2 + O + O$	2.8×10^{-11}	[24]

Table 1. (Contd.)

No.	Process	Rate constant, s^{-1}, cm^3/s, cm^6/s, $T = 323$ K	Reference
70	$N_2(E_{sum}) + O_2 \longrightarrow N_2 + O + O$	3.0×10^{-10}	[24]
71	$N_2(A^3\Sigma_u^+) + NO_2 \longrightarrow N_2 + NO + O$	1.0×10^{-12}	[24]
72	$N(^2D_0) + O_2 \longrightarrow NO + O(^3P)$	1.6×10^{-12}	[23]
73	$N(^2D_0) + O_2 \longrightarrow NO + O(^1D)$	6.2×10^{-12}	[23]
74	$N(^2D_0) + N_2 \longrightarrow N(S) + N_2$	1.5×10^{-15}	[23]
75	$O + O_2^- \longrightarrow O^- + O_2$	3.3×10^{-10}	[29]
76	$O(^1D) + N_2O \longrightarrow NO + NO$	7.2×10^{-11}	[24]
77	$O(^1D) + NO \longrightarrow O_2 + N$	8.5×10^{-11}	[24]
78	$O(^1D) + NO_2 \longrightarrow O_2 + NO$	1.4×10^{-10}	[24]
79	$O(^1D) + O_2 \longrightarrow O + O_2(b^1\Sigma)$	3.1×10^{-11}	[24]
80	$O(^1D) + O_2 \longrightarrow O + O_2$	9.3×10^{-12}	[24]
81	$O(^1D) + O_3 \longrightarrow O + O + O_2$	1.2×10^{-10}	[24]
82	$O(^1D) + N_2 \longrightarrow O + N_2$	2.5×10^{-11}	[24]
83	$O(^1D) + O_3 \longrightarrow O_2 + O_2$	2.3×10^{-11}	[24]
84	$O(^1D) + O_3 \longrightarrow O_2(a^1\Delta) + O_2$	1.5×10^{-11}	[24]
85	$O(^1D) + O_3 \longrightarrow O_2(b^1\Sigma) + O_2$	7.8×10^{-12}	[24]
86	$O(^1D) + H_2O \longrightarrow OH + OH$	2.0×10^{-10}	[24]
87	$O(^1D) + CH_4 \longrightarrow CH_3O + H$	2.5×10^{-11}	[32]
88	$O(^1D) + CH_4 \longrightarrow CH_3 + OH$	1.2×10^{-10}	[33]
89	$O_2(a^1\Delta) + O_2 \longrightarrow O_2 + O_2$	2.2×10^{-18}	[29]
90	$O_2(a^1\Delta) + N_2 \longrightarrow O_2 + N_2$	1.4×10^{-19}	[29]
91	$O_2(a^1\Delta) + H_2O \longrightarrow O_2 + H_2O$	5.6×10^{-18}	[29]
92	$O_2(b^1\Sigma) + O_2 \longrightarrow O_2 + O_2$	1.5×10^{-16}	[29]
93	$O_2(b^1\Sigma) + N_2 \longrightarrow O_2 + N_2$	2.0×10^{-15}	[29]
94	$O_2(b^1\Sigma) + O_2 \longrightarrow O_2(a^1\Delta) + O_2$	4.0×10^{-17}	[29]
95	$O_2(b^1\Sigma) + H_2O \longrightarrow O_2 + H_2O$	5.1×10^{-12}	[29]
96	$O + O + M \longrightarrow O_2 + M$	1.0×10^{-32}	[29]
97	$N_2^+ + N_2 + N_2 \longrightarrow N_4^+ + N_2$	2.6×10^{-29}	[34]
98	$N_4^+ + e \longrightarrow N_2 + N_2(E_{sum})$	3.0×10^{-7}	[35]
99	$N_2^+ + C_6H_5CH_3 \longrightarrow C_6H_5CH_3^+ + N_2$	1.6×10^{-9}	[36]
100	$N_4^+ + C_6H_5CH_3 \longrightarrow C_6H_5CH_3^+ + N_2 + N_2$	1.2×10^{-9}	[36]
101	$O_4^+ + C_6H_5CH_3 \longrightarrow C_6H_5CH_3^+ + O_2 + O_2$	1.8×10^{-9}	[36]
102	$O_2^+ + C_6H_5CH_3 \longrightarrow C_6H_5CH_3^+ + O_2$	1.8×10^{-9}	[36]
103	$O^+ + C_6H_5CH_3 \longrightarrow C_6H_5CH_3^+ + O$	1.8×10^{-9}	[36]
104	$C_6H_5CH_3^+ + e \longrightarrow C_6H_5 + CH_3$	1.0×10^{-7}	[36]
105	$C_6H_5CH_3 + e \longrightarrow C_6H_5CH_2 + H + e$	1.0×10^{-9}	[13]

* The rate constant is determined by solving the Boltzmann equation (BE) for the electron energy distribution function (EEDF). Process constants are given in the units of [s^{-1}], [cm^3/s], and [cm^6/s] for one-, two-, and three-body processes, respectively.

occurs due to the three-body and two-body ion–ion recombination. For most pairs of recombining ions, the typical temperature dependences of the constants of two-body $k_2^{ii} = 4 \times 10^{-7} (300/T)^{0.5}$ cm^3/s and three-body $k_3^{ii} = 4 \times 10^{-25} (300/T)^{2.5}$ cm^6/s interactions were used. According to [24], the recombination constants were chosen in the form $k = k_2^{ii} + Mk_3^{ii}$, where M is the concentration of the third component involved in the reaction.

As noted above, the main energy deposition into gas and the generation of active particles under conditions of [9] occurred at the plasma channel decay stage corresponding to the current pulse trailing edge. Based on the current and voltage oscillograms presented in [9], let us estimate the discharge electric field at this stage. This can be done by calculating the voltage drop at the dielectric barrier (a quartz tube with a wall thickness of 2 mm) by the displacement current density through the dielectric barrier, known from the oscillogram. Supposing that the quartz permittivity for these electric field frequencies is 4 [39], we obtain that the reduced electric field strength in the discharge at the plasma channel decay stage varies within 70–90 Td. This value is in good agreement with the results of numerical two-dimensional calculations [40] of the barrier discharge in air, in which it was found that the reduced electric field strength E/N (where N is the neutral gas density) in the microdischarge of the barrier discharge at the plasma channel decay stage, when the main energy deposition into gas occurs, does not exceed E/N = 80 Td. We also note the studies of famous researchers of the dielectric barrier discharge [41, 42], in which it was shown that most radicals and excited particles are generated in the dielectric barrier discharge at the plasma channel decay stage, rather than in the "head" of the developing streamer. At this stage, the main energy deposition into the working gas occurs. Considering all the above results, in this study, to determine the rate of the processes occurring in the discharge during collisions with electrons and resulting in generation of chemically active particles, the Boltzmann kinetic equation was numerically solved for the electron energy distribution function at the reduced electric field strength varied within E/N = 70–100 Td.

The kinetic model of plasma-chemical toluene removal in pauses between current pulses (postdischarge stage) includes ~300 reactions involving 90 components consisting of both initial substances and radicals generated in the discharge, nitrogen and oxygen atoms and molecules in ground and excited states, toluene decomposition and oxidation products. The reactions involved in plasma-chemical toluene decomposition were searched for and selected by literature sources. The first stage of toluene decomposition in the mixture $N_2 : O_2$ is the interaction of the toluene molecule with electronically excited nitrogen molecules and atoms $N_2(A^3\Sigma_u^+)$, $N_2(a'^1\Sigma_u^-)$, $N(^2D)$, and oxygen atoms. These processes lead to generation of hydrogen atoms H, radical CH_3, and aromatic ring cleavage (due to the reaction with $N_2(a'^1\Sigma_u^-)$). Hydrogen atoms generated due to fast reactions with oxygen atoms form the hydroxyl radical OH whose rate of the interaction with the toluene molecule is approximately 100 times higher than the rate of the similar interaction for oxygen atoms.

The second stage in the toluene decomposition mechanism is the interaction of its molecule with generated hydroxyl radicals and hydrogen atoms H. Due to the high rate of the hydroxyl radical OH reaction with the $C_6H_5CH_3$ molecule, even low concentrations [OH] in comparison with [O] have a significant effect on the toluene removal kinetics. The radical OH in the mixture $N_2 : O_2$ is generated in the postdischarge stage exclusively due to plasma-chemical reactions between products of initial gas mixture decomposition.

Toluene reactions with metastable nitrogen molecules and atoms have high rates and are completed in the first stage. The interaction of toluene molecules with hydroxyl radicals occurs in two channels:

(i) hydrogen atom abstraction from the side methyl group CH_3 by the radical OH;

(ii) radical OH addition to the aromatic ring.

For the conditions in nonequilibrium low-temperature plasma, the contribution of channel (i) does not exceed 10%. Therefore, the main channel of the interaction of toluene molecules with the radical OH occurs according to mechanism (ii) and results in the formation of the radical $C_6H_5OHCH_3$ which rather actively interacts with molecular oxygen. The intricate oxygen-enriched peroxide complex $C_6H_5OHOOCH_3$ formed due to this interaction is unstable and is easily destroyed during further interaction with molecular oxygen.

We note that the further stages of plasma-chemical decomposition of the generated peroxide complex have not yet been reliably experimentally confirmed and are hypothetical. In this study, we chose the dicarbonyl mechanism of peroxide aromatic complex cleavage, which is preferred by most researchers [43, 44]. The rate constants of the reactions of the peroxide aromatic complex with molecular oxygen (reactions 117, 130, and 131 in Table 2) are unknown to the authors. In numerical calculations, they varied within 10^{-15}–10^{-18} cm^3 s^{-1}. The upper limit of the variation range of the constants was chosen equal to the rate constant of reaction (69), which is reliably determined experimentally. The simulation results slightly varied as constants from this range were varied. Decomposition products of the obtained complex (carbonyls, dicarbonyls) oxidize to final products (CO, CO_2, H_2O) due to the reactions of the interaction with oxygen atoms O, hydroxyl radical OH, and radical HO_2.

Table 2. Main processes included into the postdischarge stage of the model. Process constants are given in the Arrhenius form $k = A(T/298)^n \exp(-E_a/RT)$, where $[A] = s^{-1}$ for one-body processes, $[A] = cm^3/(molecule\ s)$ for two-body processes, and $[A] = cm^6/(molecule\ s)$ for three-body processes, $[T] = K$, $[E_a] = kJ/mol$, $R = 8.31 \times 10^{-3}$ kJ/(mol K) is the universal gas constant

No.	Process	A	n	E_a	Reference
1	$N + NO_2 \longrightarrow N_2O + O$	3.0×10^{-12}	0	0	[45]
2	$N + CH_3 \longrightarrow HCN + H_2$	3.9×10^{-11}	0	3.49	[9]
3	$N + CH_4 \longrightarrow HCN + H_2 + H$	10^{-15}	0	0	[45]
4	$N + C_2H_2 \longrightarrow HCN + CH$	2.7×10^{-15}	0	0	[9]
5	$N + CH_2 \longrightarrow CN + H_2$	1.6×10^{-11}	0	0	[9]
6	$N + CH \longrightarrow CN + H$	2.1×10^{-11}	0	0	[9]
7	$N_2(A^3\Sigma_u^+) + O_2 \longrightarrow N_2O + O$	7.8×10^{-14}	0	0	[24]
8	$N_2(A^3\Sigma_u^+) + O_2 \longrightarrow O + O + N_2$	2.5×10^{-12}	0	0	[24]
9	$N_2(A^3\Sigma_u^+) + N_2O \longrightarrow N_2 + N + NO$	10^{-11}	0	0	[9]
10	$N_2(A^3\Sigma_u^+) + C_6H_5CH_3 \longrightarrow C_6H_5 + CH_3 + N_2$	6.0×10^{-11}	0	0	This study
11	$N_2(a'^1\Sigma_u^-) + C_6H_5CH_3 \longrightarrow C_5H_6 + C_2H_2 + N_2$	6.0×10^{-11}	0	0	This study
12	$N_2(A^3\Sigma_u^+) + C_6H_5CH_3 \longrightarrow C_6H_5CH_2 + H + N_2$	6.0×10^{-11}	0	0	This study
13	$N_2(A^3\Sigma_u^+) + C_6H_5CH_3 \longrightarrow C_6H_4CH_3 + H + N_2$	6.0×10^{-11}	0	0	This study
14	$N_2(E_{sum}) + O_2 \longrightarrow O + O + N_2$	3.0×10^{-10}	0	0	[46]
15	$O + NO + N_2 \longrightarrow NO_2 + N_2$	1.03×10^{-30}	−2.87	6.49	[45]
16	$O + NO_2 + N_2 \longrightarrow NO_3 + N_2$	9.02×10^{-31}	−2.0	0	[45]
17	$O + O_3 \longrightarrow O_2 + O_2$	8.0×10^{-12}	0	17.13	[45]
18	$O + H + N_2 \longrightarrow OH + N_2$	4.36×10^{-32}	−1.0	0	[45]
19	$O + CH_3 \longrightarrow CH_2O + H$	1.4×10^{-10}	0	0	[45]
20	$O + C_2H_2 \longrightarrow CO + CH_2$	3.49×10^{-12}	1.5	7.07	[45]
21	$O + C_2H_2 \longrightarrow H + HCOO$	1.5×10^{-11}	0	18.96	[45]
22	$O + CH_2O \longrightarrow OH + HCO$	1.78×10^{-11}	0.57	11.56	[45]
23	$O + CH_3O \longrightarrow OH + CH_2O$	3.0×10^{-12}	0	0	[9]
24	$O + CH_3O_2 \longrightarrow O_2 + CH_3O$	6.0×10^{-11}	0	0	[45]
25	$O + CH_3CO \longrightarrow CH_3 + CO_2$	2.56×10^{-10}	0	0	[45]
26	$O + C_6H_5CH_2 \longrightarrow C_6H_5CHO + H$	2.75×10^{-10}	0	0	[9]
27	$O + C_6H_5CH_3 \longrightarrow C_6H_5CH_2 + OH$	5.2×10^{-15}	1.21	10.7	[9]
28	$O + C_6H_5CHO \longrightarrow C_6H_5CO + OH$	1.0×10^{-11}	0	7.57	[45]
29	$O(^1D) + N_2O \longrightarrow NO + NO$	7.2×10^{-11}	0	0	[45]
30	$O(^1D) + N_2O \longrightarrow N_2 + N_2$	4.4×10^{-11}	0	0	[45]
31	$O(^1D) + O_3 \longrightarrow O_2(a^1\Delta) + O_2$	2.65×10^{-10}	0	0	[9]
32	$O(^1D) + CH_4 \longrightarrow OH + CH_3$	1.13×10^{-10}	0	0	[45]
33	$O_3 + O_2(a^1\Delta) \longrightarrow O_2 + O_2 + O$	5.2×10^{-11}	0	23.61	[45]
34	$O_3 + NO \longrightarrow NO_2 + O_2$	1.4×10^{-12}	0	10.89	[45]
35	$O_3 + H \longrightarrow OH + O_2$	1.4×10^{-10}	0	3.91	[45]
36	$O_3 + OH \longrightarrow HO_2 + O_2$	1.7×10^{-12}	0	7.82	[45]
37	$O_3 + CH_3 \longrightarrow CH_3O + O_2$	2.61×10^{-12}	0	0	[45]
38	$O_3 + HCO \longrightarrow H + CO_2 + O_2$	8.3×10^{-13}	0	0	[45]
39	$OH + CH_3 \longrightarrow H_2O + CH_2$	1.2×10^{-10}	0	11.64	[45]
40	$O_3 + CH_3 + N_2 \longrightarrow CH_3OH + N_2$	4.4×10^{-30}	−0.09	0.2	[9]

Table 2. (Contd.)

No.	Process	A	n	E_a	Reference
41	$OH + CH_4 \longrightarrow H_2O + CH_3$	6.18×10^{-13}	2.0	10.64	[45]
42	$OH + HCN \longrightarrow H_2O + CN$	1.2×10^{-13}	0	3.3	[9]
43	$OH + CH_2O \longrightarrow H_2O + HCO$	5.79×10^{-13}	2.98	−14.55	[45]
44	$OH + CH_2O \longrightarrow H + HCOOH$	2.0×10^{-13}	0	0	[45]
45	$OH + CH_3O \longrightarrow H_2O + CH_2O$	3.0×10^{-11}	0	0	[45]
46	$OH + HCOOH \longrightarrow H_2O + CO_2 + H$	4.5×10^{-13}	0	0	[45]
47	$OH + CH_3COCHO \longrightarrow H_2O + CH_3COCO$	1.5×10^{-11}	0	0	[45]
48	$OH + C_6H_5CH_3 + N_2 \longrightarrow C_6H_5OHCH_3 + N_2$	1.5×10^{-31}	0	−1.5	[9]
49	$OH + C_6H_5CH_3 \longrightarrow H_2O + C_6H_5CH_2$	2.6×10^{-13}	1.0	3.65	[9]
50	$OH + C_6H_5CHO \longrightarrow C_6H_5CO + H_2O$	1.3×10^{-11}	0	0	[9]
51	$H + HCN + N_2 \longrightarrow H_2CN + N_2$	7.75×10^{-31}	−2.73	32.09	[45]
52	$H + CH_3 + N_2 \longrightarrow CH_4 + N_2$	6.29×10^{-29}	−1.8	0	[45]
53	$H + O_2 + N_2 \longrightarrow HO_2 + N_2$	5.47×10^{-32}	−1.8	0	[45]
54	$H + CH_2O \longrightarrow H_2 + HCO$	1.44×10^{-11}	0	14.5	[45]
55	$H + CH_3O \longrightarrow H_2 + CH_2O$	3.0×10^{-11}	0	0	[45]
56	$H + CH_3O_2 \longrightarrow OH + CH_3O$	1.6×10^{-10}	0	0	[45]
57	$H + CH_3CO \longrightarrow CH_3 + HCO$	2.16×10^{-11}	0	0	[45]
58	$CH + CH \longrightarrow C_2H_2$	2.0×10^{-10}	0	0	[45]
59	$CH_2 + CH_2 \longrightarrow C_2H_2 + H + H$	2.0×10^{-10}	0	3.3	[9]
60	$CH_3 + O_2 + N_2 \longrightarrow CH_3O_2 + N_2$	3.6×10^{-31}	−2.35	5.5	[9]
61	$CH_3 + HO_2 \longrightarrow OH + CH_3O$	3.0×10^{-11}	0	0	[45]
62	$NO_2 + NO_3 + N_2 \longrightarrow N_2O_5 + N_2$	2.5×10^{-31}	−2.18	3.1	[9]
63	$NO_2 + OH + N_2 \longrightarrow HNO_3 + N_2$	2.6×10^{-30}	−2.9	0	[45]
64	$NO_2 + CH_3 \longrightarrow CH_3O + NO$	2.5×10^{-11}	0	0	[45]
65	$NO_2 + CH_3O + N_2 \longrightarrow CH_3ONO_2 + N_2$	2.81×10^{-29}	−4.5	0	[45]
66	$HO_2 + CH_2O \longrightarrow HOCH_2OO$	9.7×10^{-15}	0	−5.20	[45]
67	$O_2 + C_6H_5CH_2 \longrightarrow C_6H_5CH_2OO$	7.61×10^{-14}	0	−1.58	[45]
68	$O_2 + C_6H_5CH_2O \longrightarrow C_6H_5CHO + HO_2$	3.7×10^{-14}	0	3.8	[9]
69	$O_2 + C_6H_5OHCH_3 \longrightarrow C_6H_5OHCH_3OO$	3.7×10^{-15}	0	0	[45]
70	$CH_3O + CH_3O \longrightarrow CH_3OH + CH_2O$	1.0×10^{-10}	0	0	[45]
71	$CH_3O + CH_3O_2 \longrightarrow CH_3OOH + CH_2O$	5.0×10^{-13}	0	0	[45]
72	$HO_2 + CH_3O_2 \longrightarrow O_2 + CH_3OOH$	3.8×10^{-13}	0	−6.49	[45]
73	$CH_3 + CH_3O_2 \longrightarrow CH_3O + CH_3O$	4.0×10^{-11}	0	0	[45]
74	$HCO + CH_3O_2 \longrightarrow CH_3O + H + CO_2$	5.0×10^{-11}	0	0	[9]
75	$CH_3O_2 + CH_3O_2 \longrightarrow CH_3OH + CH_2O + O_2$	3.7×10^{-14}	0	−3.0	[9]
76	$CH_3O_2 + CH_3O_2 \longrightarrow CH_3O + CH_3O + O_2$	7.4×10^{-13}	0	4.32	[45]
77	$HOCH_2OO + HOCH_2OO \longrightarrow HCOOH + CH_2OHOH + O_2$	5.7×10^{-14}	0	−6.24	[45]
78	$C_6H_5CH_2OO + C_6H_5CH_2OO \longrightarrow C_6H_5CHO + C_6H_5CHO + O_2 + H_2$	1.38×10^{-14}	0	13.9	[9]
79	$C_6H_5CH_2OO + C_6H_5CH_2OO \longrightarrow C_6H_5CH_2O + C_6H_5CH_2O + O_2$	1.38×10^{-14}	0	13.9	[9]
80	$O + O_2 + N_2 \longrightarrow O_3 + N_2$	5.6×10^{-34}	−2.80	0	[45]
81	$O + O_2 + O_2 \longrightarrow O_3 + O_2$	6.9×10^{-34}	−1.25	0	[24]
82	$H + HCO \longrightarrow CO + H_2$	2.0×10^{-10}	0	0	[45]
83	$H + CO_2 \longrightarrow CO + OH$	2.51×10^{-10}	0	111	[45]
84	$O + CO_2 \longrightarrow CO + O_2$	2.81×10^{-11}	0	220	[45]
85	$OH + HCO \longrightarrow CO + H_2O$	5.0×10^{-11}	0	0	[45]

Table 2. (Contd.)

No.	Process	A	n	E_a	Reference
86	$O_2 + HCO \longrightarrow CO + HO_2$	5.89×10^{-12}	0	0	[45]
87	$C_6H_5 + H \longrightarrow C_6H_6$	3.65×10^{-10}	0	0	[45]
88	$H + H + N_2 \longrightarrow H_2 + N_2$	6.04×10^{-33}	0	0	[45]
89	$N_2(A^3\Sigma_u^+) + N_2(A^3\Sigma_u^+) \longrightarrow N_2(E_{sum}) + N_2$	4.5×10^{-10}	0	0	[24]
90	$C_6H_5CH_3 + H \longrightarrow C_6H_6 + CH_3$	1.35×10^{-13}	0	0	[45]
91	$C_6H_5CH_3 + N(^2D_0) \longrightarrow$ products	3.0×10^{-11}	0	0	[47]
92	$C_6H_6 + N_2(A^3\Sigma_u^+) \longrightarrow$ прproducts	1.6×10^{-10}	0	0	[45]
93	$N(^2D_0) + N_2 \longrightarrow N + N_2$	1.7×10^{-14}	0	0	[45]
94	$C_6H_5CO + O \longrightarrow C_6H_5 + CO_2$	2.32×10^{-10}	0	0	[45]
95	$C_6H_5CO + H \longrightarrow C_6H_5CHO$	4.98×10^{-11}	0	0	[45]
96	$N_2(a'^1\Sigma_u^-) + O_2 \longrightarrow O + O + N_2$	2.8×10^{-11}	0	0	[23]
97	$N + O + N_2 \longrightarrow NO + N_2$	1.0×10^{-32}	−0.5	0	[24]
98	$OH + N \longrightarrow NO + H$	4.8×10^{-11}	0	0	[24]
99	$HO_2 + O \longrightarrow OH + O_2$	2.9×10^{-11}	0	−1.7	[24]
100	$HO_2 + O_3 \longrightarrow OH + O_2 + O_2$	1.0×10^{-13}	0	10.4	[24]
101	$HO_2 + NO \longrightarrow OH + NO_2$	8.7×10^{-12}	0	−2.0	[24]
102	$N + O_2 \longrightarrow NO + O$	3.3×10^{-12}	1.0	26.0	[24]
103	$H + NO + N_2 \longrightarrow HNO + N_2$	2.1×10^{-32}	0	−2.5	[24]
104	$H + NO_2 \longrightarrow OH + NO$	8.0×10^{-11}	0	0	[24]
105	$OH + OH \longrightarrow O + H_2O$	1.0×10^{-11}	0	−4.57	[24]
106	$OH + NO + N_2 \longrightarrow HNO_2 + N_2$	6.6×10^{-31}	−2.4	0	[24]
107	$OH + NO_2 + O_2 \longrightarrow HNO_3 + O_2$	1.8×10^{-30}	−2.9	0	[24]
108	$OH + HNO_2 \longrightarrow H_2O + NO_2$	1.8×10^{-11}	0	−3.2	[24]
109	$OH + N_2O \longrightarrow HNO + NO$	3.8×10^{-17}	0	0	[24]
110	$OH + O \longrightarrow H + O_2$	2.3×10^{-11}	0	−0.9	[24]
111	$OH + HNO \longrightarrow NO + H_2O$	7.1×10^{-11}	0	0	[24]
112	$OH + H_2 \longrightarrow H_2O + H$	7.7×10^{-12}	0	8.3	[24]
113	$OH + HNO_3 \longrightarrow NO_3 + H_2O$	1.5×10^{-14}	0	−5.9	[24]
114	$O + H_2 \longrightarrow OH + H$	1.6×10^{-11}	0	38	[24]
115	$O(^1D) + H_2O \longrightarrow O + H_2O$	1.2×10^{-11}	0	0	[24]
116	$O(^1D) + H_2O \longrightarrow OH + OH$	2.2×10^{-10}	0	0	[24]
117	$C_6H_5OHCH_3OO + O_2 \longrightarrow OOC_6H_5OHCH_3OO$	8.5×10^{-16}	0	0	This study
118	$C_2H_2O_2 + OH \longrightarrow HCOOH + HCO$	7.0×10^{-12}	0	0	[48]
119	$H + HO_2 \longrightarrow H_2 + O_2$	4.2×10^{-11}	0	2.9	[24]
120	$H + OH + N_2 \longrightarrow H_2O + N_2$	4.3×10^{-31}	0	0	[24]
121	$C_6H_5CH_2 + O \longrightarrow C_6H_5 + CH_2O$	5.5×10^{-10}	0	0	[45]
122	$C_5H_5 + O \longrightarrow CO + C_4H_5$	2.4×10^{-11}	−0.28	2.0	[49]
123	$CH_3 + O \longrightarrow CH_3O$	1.22×10^{-10}	0.05	−0.57	[45]
124	$CH_3 + O \longrightarrow CO + H_2 + H$	6.0×10^{-11}	0	0	[45]
125	$C_4H_2 + O \longrightarrow CO + C_3H_2$	3.0×10^{-12}	0	0	[50]
126	$C_3H_3 + O \longrightarrow C_3H_2 + OH$	5.3×10^{-12}	0	0	[51]
127	$C_6H_5 + OH \longrightarrow C_6H_5O + H$	8.3×10^{-11}	0	0	[50]
128	$C_6H_6 + OH \longrightarrow C_6H_5 + H_2O$	2.78×10^{-14}	4.1	−1.26	[45]
129	$C_6H_6 + O \longrightarrow C_6H_5O + H$	4.0×10^{-11}	0	19.5	[52]

Table 2. (Contd.)

No.	Process	A	n	E_a	Reference
130	$OOC_6H_5OHCH_3OO + O_2 \longrightarrow CH_3COCHO + C_4H_4O_2 + HO_2 + O$	1.0×10^{-16}	0	0	This study
131	$OOC_6H_5OHCH_3OO + O_2 \longrightarrow C_2H_2O_2 + C_5H_6O_2 + HO_2 + O$	1.0×10^{-16}	0	0	This study
132	$C_2H_2O_2 + OH \longrightarrow H_2O + HCOCO$	1.1×10^{-11}	0	0	[45]
133	$C_2H_2O_2 + H \longrightarrow CO + H_2 + HCO$	5.98×10^{-14}	0	0	[45]
134	$CH_3COCO \longrightarrow CO + CH_3CO$	1.2×10^{10}	0	11.7	[45]
135	$C_4H_4O_2 + OH \longrightarrow$ products	4.5×10^{-11}	0	0	[45]
136	$C_5H_6O_2 + OH \longrightarrow$ products	5.6×10^{-11}	0	0	[45]
137	$CH_3CO \longrightarrow CH_3 + CO$	7.31×10^{12}	0	59.7	[45]
138	$CH_3CO + H \longrightarrow C_2H_2O + H_2$	1.0×10^{-11}	0	0	[45]
139	$CH_3CO + O_2 \longrightarrow CO_2 + CH_3O$	7.37×10^{-14}	0	−4.51	[45]
140	$CH_3CO + OH \longrightarrow C_2H_2O + H_2O$	2.0×10^{-11}	0	0	[45]
141	$CH_3CO + HO_2 \longrightarrow$ products	5.0×10^{-11}	0	0	[45]
142	$HCO + CH_3CO \longrightarrow CH_3CHO + CO$	1.5×10^{-11}	0	0	[45]
143	$CH_3CO + CH_3 \longrightarrow C_2H_6 + CO$	5.4×10^{-11}	0	0	[45]
144	$OH + HO_2 \longrightarrow H_2O + O_2$	1.1×10^{-10}	0	0	[45]
145	$HO_2 + HO_2 + N_2 \longrightarrow H_2O_2 + O_2 + N_2$	1.9×10^{-33}	0	−8.15	[45]
146	$OH + OH + N_2 \longrightarrow H_2O_2 + N_2$	6.9×10^{-31}	0	0	[45]
147	$HO_2 + NO_3 \longrightarrow O_2 + HNO_3$	1.9×10^{-12}	0	0	[45]
148	$O + HCO \longrightarrow H + CO_2$	5.0×10^{-11}	0	0	[45]
149	$HO_2 + HCO \longrightarrow OH + H + CO_2$	5.0×10^{-11}	0	0	[53]
150	$CH_3 + CH_3 \longrightarrow C_2H_6$	4.2×10^{-11}	0	0	[45]
151	$C_6H_5OH \longrightarrow C_5H_5 + HCO$	6.08×10^{12}	0	59.41	[45]
152	$HCOCO \longrightarrow CO + HCO$	1.4×10^{12}	0	26.27	[45]
153	$C_2H_2 + HCCO \longrightarrow CO + C_3H_3$	1.66×10^{-14}	0	0	[45]
154	$CH_3O + HCO \longrightarrow CH_3OH + CO$	2.0×10^{-10}	0	0	[45]
155	$CH_3COCHO + O(^1D) \longrightarrow$ products	9.4×10^{-13}	0	−6.49	[45]
156	$C_6H_5CHO + O \longrightarrow C_6H_4CHO + OH$	1.0×10^{-11}	0	7.57	[45]
157	$C_6H_4CHO + O \longrightarrow CO_2 + C_6H_5$	2.3×10^{-10}	0	0	[45]
158	$CH + NO \longrightarrow H + NCO$	4.0×10^{-11}	0	0	[45]
159	$O + NCO \longrightarrow CO + NO$	6.5×10^{-11}	−1.14	0	[45]
160	$H + NCO \longrightarrow CO + NH$	2.2×10^{-11}	0	0	[45]
161	$CN + NO_2 \longrightarrow NO + NCO$	8.05×10^{-11}	0	0	[45]
162	$H + HCCO \longrightarrow CO + CH_2$	1.7×10^{-10}	0	0	[45]
163	$O + HCCO \longrightarrow CO + CO + H$	1.6×10^{-10}	0	0	[45]
164	$C_2H_2 + OH \longrightarrow H_2 + HCCO$	1.91×10^{-13}	0	0	[45]
165	$CH_3COCO + O_2 \longrightarrow CH_3COCOO_2$	5.1×10^{-12}	0	0	[45]
166	$CH_3COCOO_2 \longrightarrow CO_2 + C_2H_2O + OH$	1.0×10^{2}	0	0	[45]
167	$CH_3CO + O_2 \longrightarrow CH_2O + CO + OH$	3.0×10^{-14}	0	0	[45]
168	$CH_3CO + NO_2 \longrightarrow CO_2 + CH_3 + NO$	1.66×10^{-12}	0	0	[45]
169	$C_2H_2O_2 + HO_2 \longrightarrow HCOCO + H_2O_2$	5.0×10^{-16}	0	0	[48]
170	$NCO + NCO \longrightarrow CO + CO + N_2$	5.0×10^{-12}	0	0	[45]
171	$O + CH_2 \longrightarrow CO + H + H$	1.2×10^{-10}	0	0	[45]
172	$C_2O + N \longrightarrow CN + CO$	5.5×10^{-10}	0	0	[45]
173	$C_2O + O \longrightarrow CO + CO$	8.6×10^{-11}	0	0	[45]
174	$C_2O + H \longrightarrow CO + CH$	2.2×10^{-11}	0	0	[45]
175	$NO + HCCO \longrightarrow CO + HCNO$	1.4×10^{-11}	0	−2.66	[45]

Table 2. (Contd.)

No.	Process	A	n	E_a	Reference
176	$NO + NCO \longrightarrow CO + N_2O$	3.3×10^{-11}	0	0	[45]
177	$O_2 + CH_2 \longrightarrow CO + H_2O$	4.0×10^{-13}	0	0	[45]
178	$CH + O \longrightarrow CO + H$	6.6×10^{-11}	0	0	[45]
179	$CH + NO \longrightarrow CO + NH$	2.0×10^{-10}	0	0	[45]
180	$CH + O_2 \longrightarrow CO + OH$	8.3×10^{-11}	0	0	[45]
181	$HCO + CH_2 \longrightarrow CO + CH_3$	3.0×10^{-11}	0	0	[45]
182	$HCO + NO \longrightarrow CO + HNO$	1.35×10^{-11}	0	0	[45]
183	$HCO + C_2H_3 \longrightarrow C_2H_4 + CO$	1.5×10^{-10}	0	0	[45]
184	$HCO + HCO \longrightarrow CO + CO + H_2$	3.64×10^{-11}	0	0	[45]
185	$CH_3 + HCO \longrightarrow CH_4 + CO$	4.4×10^{-11}	0	0	[45]
186	$CN + O \longrightarrow CO + N$	1.45×10^{-10}	−0.18	0	[45]
187	$CN + NO_2 \longrightarrow CO + N_2O$	7.1×10^{-12}	0	0	[45]
188	$CN + NO \longrightarrow CO + N_2$	1.6×10^{-13}	0	0	[45]
189	$C_6H_5O + O \longrightarrow C_6H_4O_2 + H$	1.4×10^{-10}	0	0	[54]
190	$C_6H_4O_2 + H \longrightarrow C_5H_5O + CO$	4.2×10^{-11}	0	19.6	[54]
191	$C_6H_4O_2 + O \longrightarrow C_6H_3O_3 + H$	2.5×10^{-11}	0	18.9	[54]
192	$C_6H_3O_3 + H \longrightarrow C_2H_2 + C_2H_2O + CO + CO$	1.6×10^{-10}	0	0	[54]
193	$C_6H_4O_2 + H \longrightarrow C_6H_3O_2 + H_2$	3.3×10^{-12}	0	13.4	[54]
194	$C_6H_4O_2 + OH \longrightarrow C_6H_3O_2 + H_2O$	1.5×10^{-13}	2.0	16.7	[54]
195	$C_6H_4O_2 + O \longrightarrow C_6H_3O_2 + OH$	2.3×10^{-11}	0	61	[54]
196	$C_6H_3O_2 + H \longrightarrow C_2H_2 + C_2H_2 + CO + CO$	1.6×10^{-10}	0	0	[55]
197	$C_6H_3O_2 + O \longrightarrow C_2H_2 + HCCO + CO + CO$	1.6×10^{-10}	0	0	[55]
198	$C_6H_5OH + OH \longrightarrow C_6H_5O + H_2O$	4.35×10^{-13}	2.0	−5.49	[45]
199	$C_6H_5CH_2 + HO_2 \longrightarrow C_6H_5 + CH_2O + OH$	8.3×10^{-12}	0	0	[45]
200	$C_6H_5 + O \longrightarrow C_5H_5 + CO$	1.5×10^{-10}	0	0	[56]
201	$C_4H_5 + H \longrightarrow C_4H_6$	1.51×10^{-10}	0.2	−0.48	[45]
202	$C_4H_5 + H_2 \longrightarrow C_4H_6 + H$	1.14×10^{-13}	0.5	15.46	[45]
203	$C_4H_6 + O \longrightarrow CO + C_3H_6$	9.96×10^{-11}	0	7.48	[45]
204	$C_6H_5 + CH_2O \longrightarrow C_6H_6 + HCO$	3.72×10^{-14}	2.19	0.16	[45]
205	$C_6H_5O + O \longrightarrow C_5H_5 + CO_2$	1.7×10^{-11}	0	0	[54]
206	$C_2H_2O + H \longrightarrow CO + CH_3$	6.19×10^{-14}	0	0	[45]
207	$C_2H_2O + OH \longrightarrow CO + CH_3O$	1.0×10^{-11}	0	0	[45]
208	$C_2H_2O + CH_2 \longrightarrow C_2H_4 + CO$	2.09×10^{-10}	0	0	[45]
209	$HOCH_2OO + HO_2 \longrightarrow O_2 + HCOOH + H_2O$	3.6×10^{-12}	0	0	[45]
210	$C_4H_4 + C_2H \longrightarrow C_4H_3 + C_2H_2$	6.6×10^{-11}	0	0	[57]
211	$C_4H_3 + O \longrightarrow C_2H_2O + C_2H$	3.0×10^{-11}	0	0	[50]
212	$C_4H_3 + O_2 \longrightarrow C_2H_2O + HCOO$	1.7×10^{-12}	0	0	[50]
213	$C_4H_3 + OH \longrightarrow C_4H_2 + H_2O$	5.0×10^{-11}	0	0	[50]
214	$C_4H_3 + H \longrightarrow C_4H_2 + H_2$	4.2×10^{-11}	0	0	[50]
215	$C_2H_2O + O \longrightarrow HCO + HCO$	3.4×10^{-11}	0	9.6	[58]
216	$C_2H_2O + O \longrightarrow CH_2 + CO_2$	2.9×10^{-12}	0	5.6	[58]
217	$C_2H_2O + O \longrightarrow CH_2O + CO$	3.3×10^{-11}	0	0	[58]
218	$C_2H_2 + OH \longrightarrow C_2H_2O + H$	1.0×10^{-13}	0	0	[45]
219	$C_4H_2 + OH \longrightarrow HCO + C_3H_2$	5.0×10^{-12}	0	0	[58]
220	$C_4H_2 + O \longrightarrow HCCO + C_2H$	1.6×10^{-11}	0	0	[58]
221	$C_4H_4 + H \longrightarrow C_4H_3 + H_2$	3.0×10^{-11}	2	62.7	[50]

Table 2. (Contd.)

No.	Process	A	n	E_a	Reference
222	$C_4H_4 + OH \longrightarrow C_4H_3 + H_2O$	1.1×10^{-12}	2	20.7	[50]
223	$C_6H_5OH + C_4H_5 \longrightarrow C_6H_5O + C_4H_6$	1.0×10^{-11}	0	0	[59]
224	$C_4H_4O_2 + OH \longrightarrow C_3H_4O + COOH$	5.2×10^{-11}	0	0	[48]
225	$C_3H_4O \longrightarrow C_2H_4 + CO$	1.0×10^{9}	0	0	[45]
226	$C_4H_4O_2 + OH \longrightarrow C_2H_2O + C_2H_3O_2$	5.2×10^{-11}	0	0	[48]
227	$C_2H_3O_2 \longrightarrow CO_2 + CH_3$	5.3×10^{3}	0	0	[45]
228	$COOH + O_2 \longrightarrow CO_2 + HO_2$	2.1×10^{-12}	0	0	[45]
229	$C_2H_2 + COOH \longrightarrow CO_2 + C_2H_3$	3.0×10^{-14}	0	0	[45]
230	$C_2H_4 + COOH \longrightarrow CO_2 + C_2H_5$	1.0×10^{-14}	0	0	[45]
231	$COOH + O \longrightarrow CO_2 + OH$	1.44×10^{-11}	0	0	[45]
232	$COOH + OH \longrightarrow CO_2 + H_2O$	1.0×10^{-11}	0	0	[45]
233	$C_2H_2O_2 + OH \longrightarrow CO + HCO + H_2O$	7.0×10^{-12}	0	0	[48]
234	$C_2H_2O_2 + H \longrightarrow H_2 + HCOCO$	5.98×10^{-14}	0	0	[48]
235	$C_2H_2O_2 + H \longrightarrow CH_2O + HCO$	5.98×10^{-14}	0	0	[48]
236	$C_2H_2O_2 + HO_2 \longrightarrow HCO + CH_2O_3$	5.0×10^{-16}	0	0	[48]
237	$C_2H_2O_2 + HO_2 \longrightarrow HCO + H_2O_2 + CO$	5.0×10^{-16}	0	0	[48]
238	$C_6H_5CHO + OH \longrightarrow$ products	1.4×10^{-11}	0	0	[45]
239	$CH_3O + O_2 \longrightarrow CH_2O + HO_2$	9.6×10^{-12}	0	0	[45]
240	$CH_3 + O \longrightarrow CH_2O + H$	1.4×10^{-10}	0	0	[45]
241	$CH_3 + OH \longrightarrow CH_2O + H_2$	1.7×10^{-12}	0	0	[45]
242	$CH_3O + NO_3 \longrightarrow CH_2O + HNO_3$	1.5×10^{-12}	0	0	[45]
243	$CH_4 + O(^1D) \longrightarrow CH_2O + H_2$	1.5×10^{-11}	0	0	[45]
244	$C_2H_4 + O \longrightarrow CH_3 + HCO$	1.5×10^{-12}	1.55	1.79	[45]
245	$C_2H_4 + O \longrightarrow CH_2O + CH_2$	9.7×10^{-14}	0	0	[45]
246	$C_2H_4 + OH \longrightarrow CH_3 + CH_2O$	1.66×10^{-12}	0	−3.8	[53]
247	$HCO + HCO \longrightarrow CH_2O + CO$	4.48×10^{-11}	0	0	[45]
248	$C_4H_6 + O \longrightarrow C_3H_4 + CH_2O$	1.7×10^{-12}	0	0	[60]
249	$C_4H_6 + OH \longrightarrow C_3H_5 + CH_2O$	1.7×10^{-12}	0	0	[60]
250	$HNO_2 + O_3 \longrightarrow HNO_3 + O_2$	5.0×10^{-19}	0	0	[45]
251	$H_2O_2 + NO_3 \longrightarrow HO_2 + HNO_3$	2.0×10^{-15}	0	0	[45]
252	$CH_3CHO + NO_3 \longrightarrow CH_3CO + HNO_3$	2.1×10^{-15}	0	0	[45]
253	$HNO_2 + O \longrightarrow HNO_3$	1.0×10^{-15}	0	0	[45]
254	$CH_3O_2 + NO \longrightarrow CH_3ONO_2$	3.0×10^{-13}	0	0	[45]
255	$C_2H_3O_2 \longrightarrow CO + CH_3O$	3.0×10^{4}	0	0	[45]
256	$C_2H_3O_2 + CH_3O \longrightarrow CH_2O + C_2H_4O_2$	3.79×10^{-11}	0	0	[45]
257	$CH_3O + NO_2 \longrightarrow CH_3ONO_2$	2.41×10^{-11}	−0.88	0	[45]
258	$C_4H_4 + O \longrightarrow CH_2O + C_3H_2$	4.98×10^{-11}	0	7.57	[48]
259	$C_4H_5 + O_2 \longrightarrow C_4H_4 + HO_2$	2.0×10^{-13}	0	0	[59]
260	$C_3H_2 + O \longrightarrow C_2H + HCO$	1.1×10^{-10}	0	0	[51]
261	$C_3H_2 + O \longrightarrow C_2H_2 + CO$	1.7×10^{-10}	0	0	[50]
262	$C_3H_2 + OH \longrightarrow C_2H_2 + HCO$	8.3×10^{-11}	0	0	[50]
263	$C_2H_2 + OH \longrightarrow C_2H + H_2O$	5.0×10^{-12}	2	58.5	[50]
264	$C_2H_2 + O \longrightarrow C_2H_2O$	2.16×10^{-13}	0	0	[45]
265	$O_2 + HOCH_2O \longrightarrow H_2O + HCOOH$	3.5×10^{-14}	0	0	[45]
266	$HOCH_2OO + HOCH_2OO \longrightarrow HOCH_2O + HOCH_2O + O_2$	5.5×10^{-12}	0	0	[45]

Simultaneously with the channel described above, there exists the other mechanism of toluene decomposition, associated with the hydrogen atom abstraction from the methyl group, which results in benzyl $C_6H_5CH_2$ generation. The radical $C_6H_5CH_2$ interacts with atoms O and radicals HO_2 with the formation of benzaldehyde C_6H_5CHO and with molecular oxygen with the formation of the peroxide radical $C_6H_5CH_2OO$. The obtained products are efficiently oxidized by atoms O, radicals OH, HO_2, and molecular oxygen O_2 to C_6H_5CO and then to C_6H_5 and CO_2. The transformation channels of the phenyl radical C_6H_5 are currently studied in sufficient detail in connection with the benzene oxidation problem.

In experiments on plasma-chemical toluene decomposition, nonvolatile products of dark brown color are always observed in the form of deposits on electrode elements and gas-discharge chamber walls [9]. A chemical analysis of these products shows that their composition contains cresols, nitrobenzene, bibenzyl, polyaromatic molecules, and others. Experimental studies show that deposits on electrodes and walls appear only during long-term operation of a plasma-chemical reactor. Estimations using the experimental data [3] show that no more than 5% of removed toluene transform to nonvolatile products. In the present model, these toluene transformation channels are disregarded.

The list of reactions included in the toluene transformation mechanisms described above is given in Table 2. Reverse reactions are neglected in the developed model. This is mainly due to the absence of data on thermodynamic functions of most intermediate products of toluene decomposition. Estimations of the possible effect of reverse reactions on the toluene removal efficiency showed that their role is insignificant at a gas temperature of 323 K. In what follows, all references to reaction number relate to Table 2.

One of the objectives of this study is to determine the role of metastable electronically excited nitrogen molecules and atoms in the plasma-chemical mechanism of toluene decomposition. The experimental results of [9, 10] show a rather high efficiency of $C_6H_5CH_3$ decomposition in nitrogen gas-discharge plasma. Performance of experiments on toluene removal under ultimately simplified experimental conditions, in which the number of active components is small and the results obtained can be unambiguously interpreted, is very important, since it allows the most reliable identification of $C_6H_5CH_3$ conversion channels and the choice of rate constants of the main reactions. Furthermore, as noted above, molecular nitrogen is a main component of the most polluted gas flows into which a significant fraction of the deposited gas-discharge energy comes; therefore, there is reason to believe that excited nitrogen appreciably contributes to toluene decomposition under these conditions as well. Taking into account the importance of electronically excited nitrogen as a reservoir of the stored internal energy, we dwell on the features of its interaction with toluene.

The list of the main reactions describing the plasma-chemical model of toluene decomposition in pure nitrogen plasma consists of processes (10)–(13), (90), and (91). As a basis of the kinetic model, the processes involving toluene, presented in [9], were taken. In this list, first of all, attention should be paid to the reactions of metastable electronically excited nitrogen $N_2(A^3\Sigma_u^+)$ and $N_2(a'^1\Sigma_u^-)$ molecules with toluene (10–13), from which toluene conversion begins and which mainly contribute to toluene removal. It should be noted that the reaction $N_2(A^3\Sigma_u^+)$ with the other aromatic hydrocarbon, benzene C_6H_6 [60, 61], is currently experimentally studied,

$$N_2\left(A^3\Sigma_u^+\right) + C_6H_6 \rightarrow \text{products},$$

and we know of no direct experimental confirmations of reactions (10)–(13). Inclusion of reactions (10)–(13) into the toluene decomposition mechanism is based on the known experimental fact that the rate of the reaction of $N_2(A^3\Sigma_u^+)$ state quenching by hydrocarbons of the same homologous series increases as they are complicated. The presence of methane CH_4 and cyanic hydrogen HCN in toluene decomposition byproducts counts in favor of reactions (10), (12), and (13) in which H atoms and methyl groups CH_3 are generated. The relative probability of reactions (10), (12), and (13) can be estimated from their exothermic effect. It seems that reaction (12), whose exothermic effect of 2.3 eV is maximum, has the highest probability. Reactions (10) and (13) have approximately identical probabilities, since their exothermic effects are close and equal to 1.7 and 1.3 eV, respectively. However, the differences between the rate constants of reactions (10) and (13), on one hand, and reaction (12), on the other hand, should not be significant, since all these reactions are strongly exothermic. In our calculations, the rate constants are taken equal to each other. Generation of an appreciable acetylene C_2H_2 amount at the plasma-chemical reactor output suggests that $C_6H_5CH_3$ conversion is accompanied by reactions with benzene ring cleavage. In [9], the following reaction is proposed

$$N_2\left(A^3\Sigma_u^+\right) + C_6H_5CH_3 \rightarrow C_5H_6 + C_2H_2 + N_2.$$

However, despite the fact that the electronic energy store of the $N_2(A^3\Sigma_u^+)$ molecule is sufficient to overcome the reaction energy barrier, an analysis of initial and final products of this reaction shows its low probability due to spin nonconservation. In this study, as a reaction with benzene ring cleavage, reaction (11) is proposed, in which the nitrogen molecule in the metastable triplet state $N_2(A^3\Sigma_u^+)$ is substituted with the

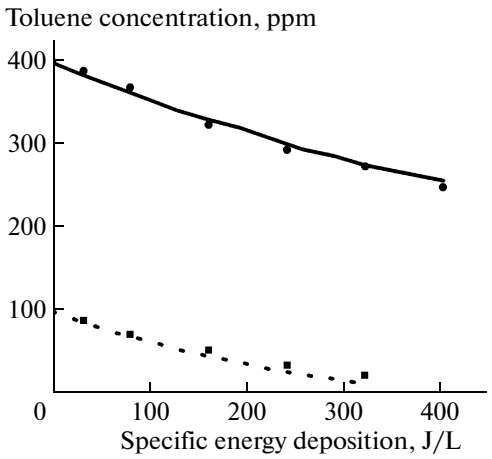

Fig. 1. Dependence of the toluene concentration at the reactor output on the specific energy deposition at $[C_6H_5CH_3]_0 = 100$ ppm (squares) and 400 ppm (circles) for $T = 323$ K. The symbols show the experimental data [9], and the solid and dashed curves are the simulation results for 400 and 100 ppm, respectively.

molecule in the metastable singlet state $N_2(a'^1\Sigma_u^-)$ with the rate constant equal to the rate constant of reactions (10), (12), and (13). The magnitudes of the rate constants of reactions (10)–(13) are taken equal to $0.25k_b$, where k_b is the rate constant of $N_2(A^3\Sigma_u^+)$ with benzene. The reactions of $C_6H_5CH_3$ molecules with hydrogen H (90) and nitrogen N (91) atoms make a noticeably smaller contribution to toluene removal in comparison with reactions (10)–(13): their contribution does not exceed 10 and 5%, respectively. However, their inclusion into the toluene conversion mechanism improves agreement of numerical simulation results with experimental data. The contribution of ion–molecule reactions to toluene removal does not exceed 0.5% of the contribution of reactions (10)–(13). Pooling reactions (89) have a significant effect on the balance of $N_2(A^3\Sigma_u^+)$ molecules only at low toluene concentrations.

Numerical calculations were performed using the Chemical Workbench program [63] which allows simultaneous solution of chemical and ion–molecule kinetic equations, the Boltzmann equation for the electron energy distribution function, and equations for gas translational temperature.

3. NUMERICAL SIMULATION RESULTS, COMPARISON WITH THE EXPERIMENT

3.1. Plasma-Chemical Toluene Decomposition in Pure Nitrogen

The main primary channels of toluene decomposition, initiated by nitrogen plasma, are associated with $C_6H_5CH_3$ reactions with metastable electronically excited $N_2(A^3\Sigma_u^+)$ and $N_2(a'^1\Sigma_u^-)$ molecules. Hydrogen and nitrogen atoms make an insignificant contribution to $C_6H_5CH_3$ removal. Below we present these reactions

$$N_2\left(A^3\Sigma_u^+\right) + C_6H_5CH_3 \rightarrow C_6H_5 + CH_3 + N_2, \quad (10)$$

$$N_2\left(a'^1\Sigma_u^-\right) + C_6H_5CH_3 \rightarrow C_5H_6 + C_2H_2 + N_2, \quad (11)$$

$$N_2\left(A^3\Sigma_u^+\right) + C_6H_5CH_3 \rightarrow C_6H_5CH_2 + H + N_2, \quad (12)$$

$$N_2\left(A^3\Sigma_u^+\right) + C_6H_5CH_3 \rightarrow C_6H_4CH_3 + H + N_2, \quad (13)$$

$$H + C_6H_5CH_3 \rightarrow C_6H_6 + CH_3, \quad (90)$$

$$N(^2D) + C_6H_5CH_3 \rightarrow C_6H_5CH_2 + NH. \quad (91)$$

A comparison of numerical simulation results with experimental data [9] was performed by the degree of toluene removal and by-product composition and concentrations, depending on the energy deposition to the discharge at various reduced electric fields in the range $E/N = 70$–100 Td. Figure 1 shows the comparison of the numerical calculation results and experimental data [9] on $C_6H_5CH_3$ removal as a function of the energy deposition at two initial toluene concentrations. Numerical calculations showed that the simulation results reproduce experimental data with good accuracy at $E/N = 70$ Td.

Figure 2 shows the calculated dynamics of the toluene concentration in the postdischarge stage of the second current pulse. There are also given the concentrations of $N_2(A^3\Sigma_u^+)$, $N_2(a'^1\Sigma_u^-)$, and hydrogen atoms H. These particles control the main channels of $C_6H_5CH_3$ decomposition (nitrogen atoms N make a significantly smaller contribution). As can be seen from the results presented, the toluene decomposition dynamics includes two characteristic stages: the fast one (characteristic time is ≈5 μs) during which most toluene is removed, and the slow stage with a characteristic time of ≈100 ms which makes a significantly smaller contribution to $C_6H_5CH_3$ decomposition.

A comparison of the toluene decomposition dynamics with the behavior of the main active components of nitrogen (Fig. 2) shows that all active molecular nitrogen components are expended at the stage of fast removal (to 5 μs).

Slow toluene removal at times $t > 5$ μs is mostly caused by hydrogen atoms generated in reaction (90). We can see in Fig. 2 that more than 95% of generated $N_2(A^3\Sigma_u^+)$ and $N_2(a'^1\Sigma_u^-)$ molecules are expended to toluene molecule decomposition at an initial toluene concentration of 400 ppm, while pooling reaction (89) has an insignificant effect on the $N_2(A^3\Sigma_u^+)$ balance. The numerically calculated energy expenditure ε for one toluene molecule removal is ε ≈ 1150 eV/mole-

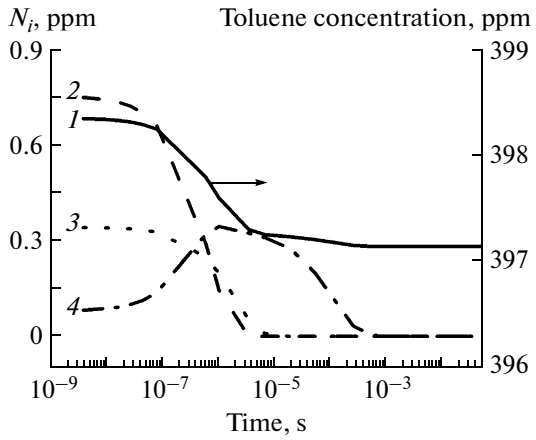

Fig. 2. Calculated temporal dynamics of toluene and active nitrogen components in the postdischarge stage of the second current pulse at the initial toluene concentration is $[C_6H_5CH_3]_0 = 400$ ppm, gas temperature $T = 323$ K, and specific energy deposition $Q = 3.25$ J/L: (*1*) toluene, (*2*) $N_2(A^3\Sigma_u^+)$, (*3*) $N_2(a'^1\Sigma_u^-)$, and (*4*) H.

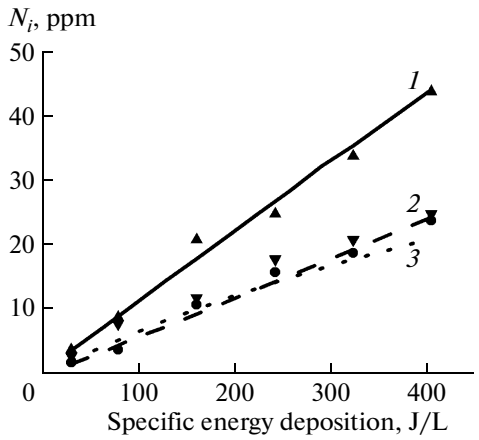

Fig. 3. Dependence of the concentration of by-products at the reactor output on the specific energy deposition at $[C_6H_5CH_3]_0 = 400$ ppm and $T = 323$ K: (*1*) C_2H_2 (triangles and solid curves), (*2*) HCN (inverted triangles and dashed curves), and (*3*) CH_4 (circles and dotted curves). The symbols show the experimental data [9], and the curves show the simulation results.

cule. This value is rather close to the experimentally measured one, $\varepsilon \approx 1200$ eV/molecule [9].

Figure 3 shows the results of numerical simulation of generation of some toluene decomposition by-products at the initial concentration $[C_6H_5CH_3]_0 = 400$ ppm and their comparison with experimental data. We can see good enough agreement of calculated and experimental data [9].

Among the results shown in Fig. 3, first of all, noteworthy is the linear increase in acetylene C_2H_2 with energy deposition. Such C_2H_2 behavior suggests that reactions with benzene ring cleavage efficiently occur in nitrogen gas-discharge plasma and produced acetylene weakly decays in the discharge. An analysis of the calculated dynamics of the increase in C_2H_2 in the postdischarge stage of each current pulse shows that the increase in the acetylene concentration correlates well with the fast $C_6H_5CH_3$ decomposition stage. The found correlation counts in favor of the fact that reaction (11) proposed in the model, which occurs with benzene ring cleavage and leading to the rapid formation of C_2H_2, actually occurs. Other acetylene production reactions (58) and (59) under the experimental conditions of [9] have substantially lower rates. Similar conclusions can also be made with respect to methane. The main channel of CH_4 production is related to reaction (52) between toluene decomposition products H and CH_3 generated in reactions (10), (12), and (13). This means that the proposed scheme of toluene decomposition by metastable $N_2(A^3\Sigma_u^+)$ molecules corresponds to actual processes. According to the experiment, the kinetic model predicts cyanic hydrogen HCN generation during toluene decomposition in nitrogen plasma. This substance is rather toxic; therefore, its generation is strongly discouraged in gas purification technologies. An analysis of the HCN production and decomposition kinetics within the developed model allowed the determination of purification conditions under which the HCN yield is completely suppressed.

3.2. Toluene Decomposition and Oxidation in the Mixture of Molecular Nitrogen and Oxygen

In the gas mixture $N_2 : O_2$, to toluene decomposition reactions (10)–(13) in nitrogen plasma, the following channels are added

$$O + C_6H_5CH_3 \rightarrow C_6H_5CH_2 + OH, \quad (27)$$

$$OH + C_6H_5CH_3 + N_2 \rightarrow C_6H_5CH_3OH + N_2, \quad (48)$$

$$OH + C_6H_5CH_3 \rightarrow C_6H_5CH_2 + H_2O. \quad (49)$$

We note that the initial gas mixture does not contain water vapor H_2O; therefore, the hydroxyl radical OH is generated in plasma-chemical reactions between toluene decomposition products and oxygen atoms. The main channel of the hydroxyl radical OH generation is reaction (18)

$$O + H + N_2 \rightarrow OH + N_2. \quad (18)$$

The radical OH, in addition to reaction (18), is also generated in a number of reactions between products of plasma-chemical transformations (see Table 2); however, reaction (18), according to numerical calculation results, does make the main contribution to OH generation.

The degree of plasma ionization in the dielectric barrier discharge in the gas mixture $N_2 : O_2$ at atmospheric pressure is in the range of 10^{-7}–10^{-6} [22]. In

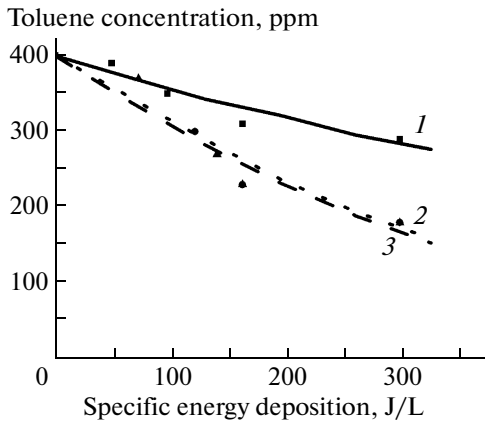

Fig. 4. Dependence of the toluene concentration at the plasma-chemical reactor output on the specific energy deposition at various oxygen contents in the gas mixture at the initial toluene concentration $[C_6H_5CH_3]_0 = 400$ ppm and gas temperature $T = 323$ K: (*1*) 0% O_2 (squares and solid curves), (*2*) 1.5% O_2 (circles and dashed curves), and (*3*) 10% O_2 (triangles and dotted curves). The symbols show the experimental data [9], and the curves show the simulation results.

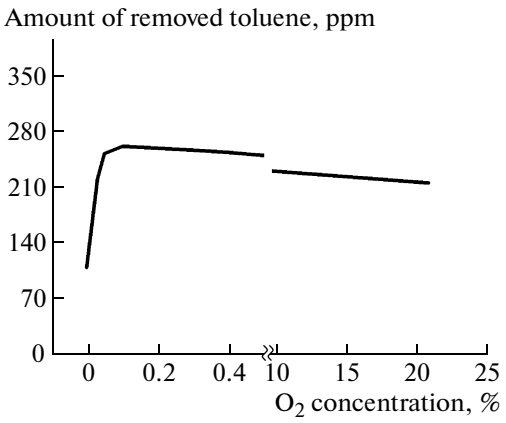

Fig. 5. Dependence of the toluene removal efficiency on the oxygen content in the gas mixture at the initial concentration $[C_6H_5CH_3]_0 = 400$ ppm, gas temperature $T = 323$ K, and specific energy deposition $Q = 325$ J/L.

this case, as calculations showed, ion–molecule reactions, as the direct electron impact, have no appreciable effect on the toluene decomposition mechanism.

Figure 4 shows the results of numerical simulation of the degree of toluene removal as a function of the energy deposition in the gas mixture $N_2 : O_2$ at three oxygen concentrations $[O_2] = 0\%$ (pure nitrogen), 1.5%, and 10% and the initial toluene concentration of 400 ppm. For comparison, the experimental results [9] are also presented.

We can see that the numerical simulation results reproduce the experimental data with good accuracy. However, it should be noted that, to achieve agreement between numerical simulation and experimental results on the degree of toluene removal at the oxygen concentration $[O_2] = 10\%$, the reduced electric field in the plasma channel of the secondary streamer (where, according to the model, chemically active particles are mostly generated) should be increased from 70 Td (pure nitrogen and mixture $N_2 : O_2$ with $[O_2] = 1.5\%$) to 80 Td. This value of E/N is in good agreement with the results of [40]. The energy expenditure of one toluene molecule removal in the presence of oxygen in the gas mixture significantly decreases in comparison with pure nitrogen and, at $[O_2] = 1.5$ and 10%, is 350 eV/molecule.

Figure 5 shows the numerical simulation results showing the dependence of the toluene removal efficiency on the oxygen percentage in the gas mixture at a fixed energy deposition to gas. At first sight, the results obtained seem rather unexpected.

It is easily seen from the results presented that the model predicts the nonmonotonic dependence of the toluene removal efficiency on the oxygen concentration $[O_2]$, i.e., there is an optimum concentration $[O_2]_{opt}$ at which the amount of removed toluene is maximum. The energy expenditure of one toluene molecule removal at the optimum concentration $[O_2]$ ($[O_2]_{opt} = 0.1\%$ at $[C_6H_5CH_3]_0 = 400$ ppm) decreases from 350 eV/molecule at $[O_2] = 10\%$ to 230 eV/molecule. In [9], the experiments on toluene removal were performed only at $[O_2] = 0$, 1.5, and 10%; in this case, the $C_6H_5CH_3$ removal efficiency appeared almost identical at $[O_2] = 1.5$ and 10% (Fig. 4); therefore, no optimum oxygen concentration $[O_2]_{opt}$ was detected. At the same time, it was experimentally shown in [10] that the efficiency of toluene removal in the BD in the gas mixture $N_2 : O_2$ at $[O_2] = 2\%$ is higher than at $[O_2] = 20\%$. We note that in [10], the amount of removed $C_6H_5CH_3$ in pure nitrogen ($[O_2] = 0\%$) was also higher than in dry air ($[O_2] = 20\%$). Based on the results obtained, it was assumed in [10] that the oxygen concentration $[O_2] = 2\%$ is optimum for toluene removal. It should be noted that, unlike [10], in [9] and our numerical calculations (Fig. 5), the oxygen additive to nitrogen always leads to an increase in the toluene removal efficiency.

The effect of molecular oxygen on the toluene removal efficiency can occur in several channels. Since oxygen, in contrast to nitrogen, is an electronegative gas, the oxygen additive to the initial gas mixture leads to the formation of additional electron loss channels and the formation of new ion types in plasma. If the oxygen content exceeds a certain level, these effects can result in a change in discharge characteristics. In [9], it is stated that the discharge characteristics depend weakly on the gas medium composition. At the same time, in [64], where the effect of the

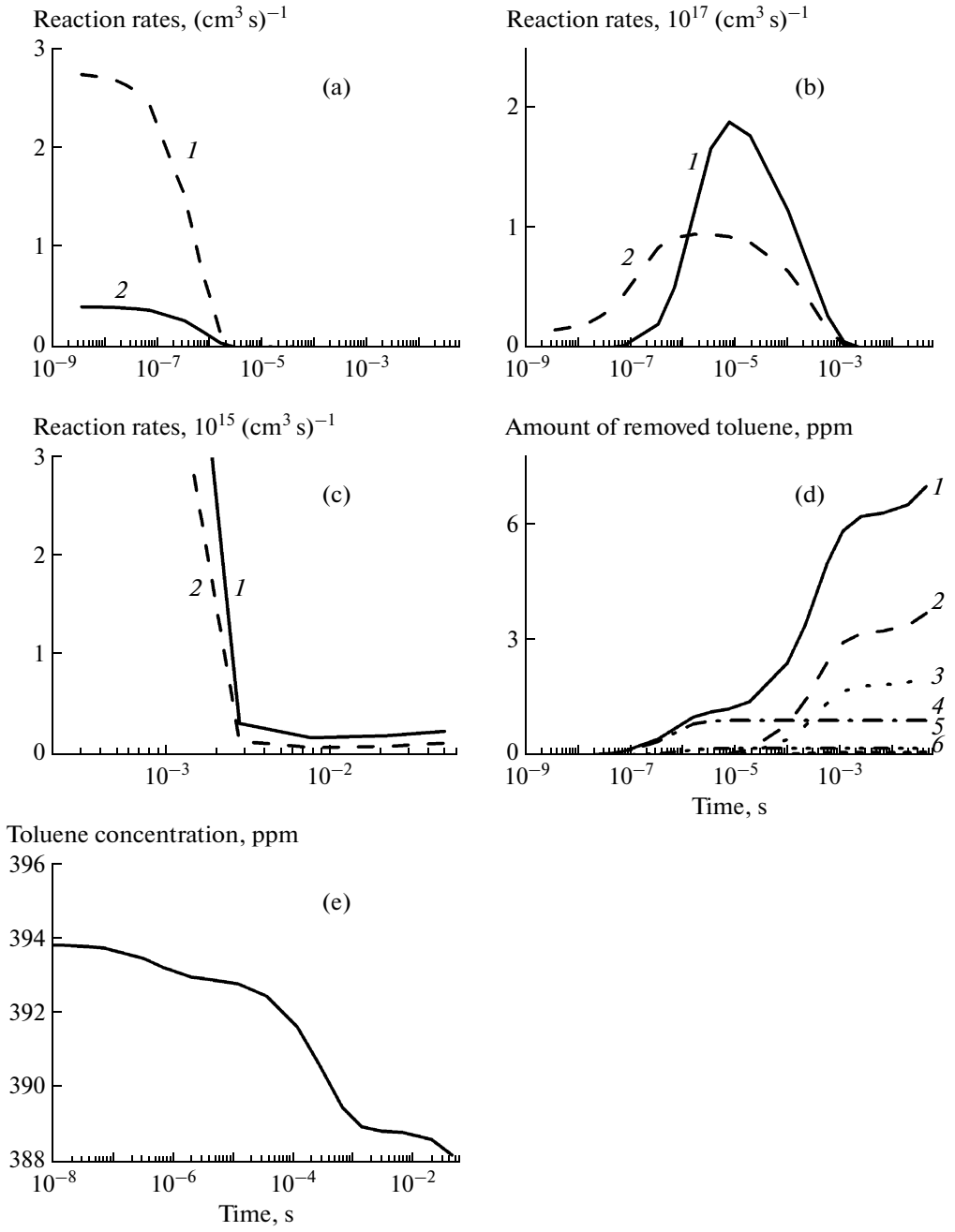

Fig. 6. Dynamics of $C_6H_5CH_3$ decomposition and oxidation after the discharge stage of the second current pulse in the $N_2 : O_2$ mixture at $[O_2] = 0.1\%$, initial toluene concentration $[C_6H_5CH_3]_0 = 400$ ppm, gas temperature $T = 323$ K, and specific energy deposition $Q = 3.25$ J/L. The toluene decomposition reaction rates in (a) (*1*) reactions (10), (12), and (13) and (*2*) reaction (11); (b, c) (*1*) reaction (48) and (*2*) reaction (27). Plot (d) shows the contributions of individual channels of toluene decomposition to total $C_6H_5CH_3$ removal: (*1*) total $C_6H_5CH_3$ removal; (*2*) reaction (48); (*3*) reaction (27); (*4*) reactions (10), (12), and (13); (*5*) reaction (11); and (*6*) reaction (90). Plot (e) shows the $C_6H_5CH_3$ concentration dynamics in the postdischarge stage of the second current pulse in the mixture $N_2 : O_2$ at $[O_2] = 0.1\%$.

concentration $[O_2]$ on microdischarge characteristics in the dielectric barrier discharge was studied at an applied sinusoidal voltage with a frequency of 1 kHz, it was found that a molecular oxygen additive of 2% to pure nitrogen has no appreciable effect on MD characteristics; however, at 10% O_2, this effect becomes noticeable. In the present study, as noted above, to fit the numerical simulation results to the experimental data at an oxygen concentration of 10%, the reduced electric field strength in the discharge should be

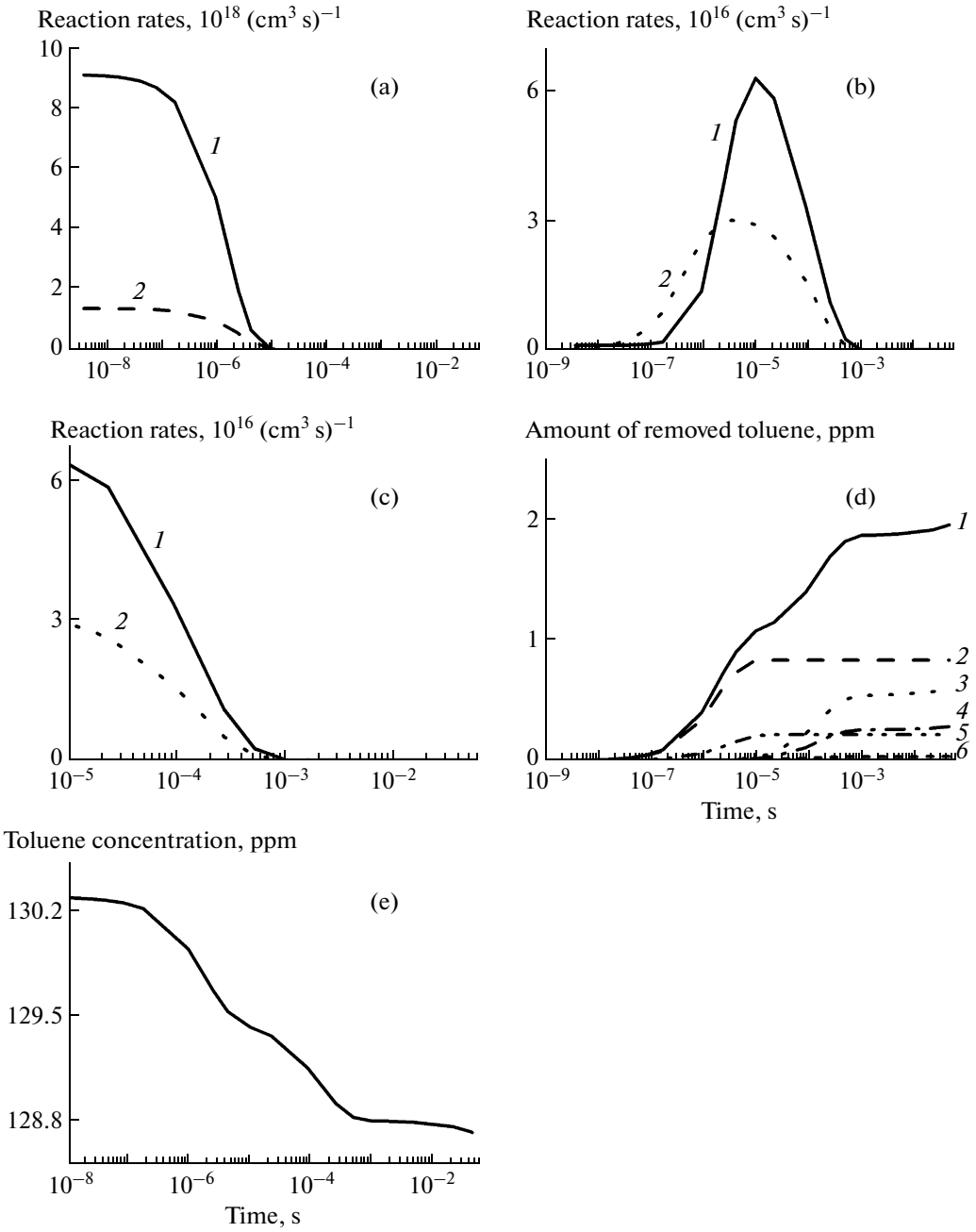

Fig. 7. The same as in Fig. 6, but for the 100th current pulse.

increased from 70 to 80 Td. As seen in Fig. 5, the oxygen concentration $[O_2]_{opt}$ at which the maximum efficiency of $C_6H_5CH_3$ removal is observed does not exceed 1%; hence, the effect of oxygen on the toluene removal efficiency is unrelated to changes in discharge characteristics.

The other channel of the effect of oxygen on the toluene removal efficiency is associated with a change in the kinetics of plasma-chemical reactions of $C_6H_5CH_3$ decomposition as O_2 is added. To determine changes in the plasma-chemical reaction mechanism with increasing concentration $[O_2]$, the kinetic dependences of the rates of main $C_6H_5CH_3$ removal channels in each current pulse were analyzed, their evolution with $[O_2]$ was determined, and the contributions of these channels to the total degree of toluene decomposition were calculated. As an example, Fig. 6 shows the kinetic curves showing the temporal dynamics of main channels of toluene decomposition (Figs. 6a–6c), the contribution of each channel to the total amount of removed toluene (Fig. 6d), and the dynamics of the $C_6H_5CH_3$ concentration (Fig. 6e) in the

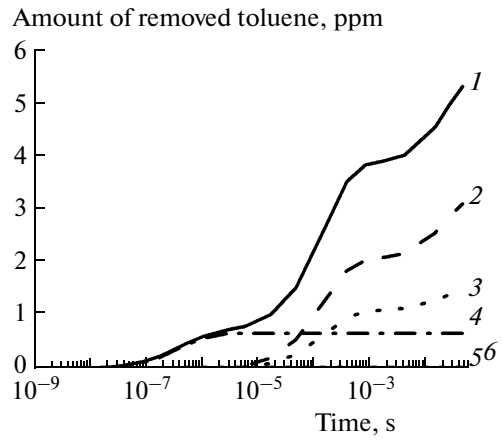

Fig. 8. Contributions of individual $C_6H_5CH_3$ decomposition channels to the total amount of removed toluene in the postdischarge stage of the second current pulse at the oxygen concentration $[O_2] = 1.5\%$, initial toluene concentration $[C_6H_5CH_3]_0 = 400$ ppm, gas temperature $T = 323$ K, and specific energy deposition $Q = 3.25$ J/L: (*1*) total $C_6H_5CH_3$ removal; (*2*) reaction (48); (*3*) reaction (27); (*4*) reactions (10), (12), and (13); (*5*) reaction (11); and (*6*) reaction (90).

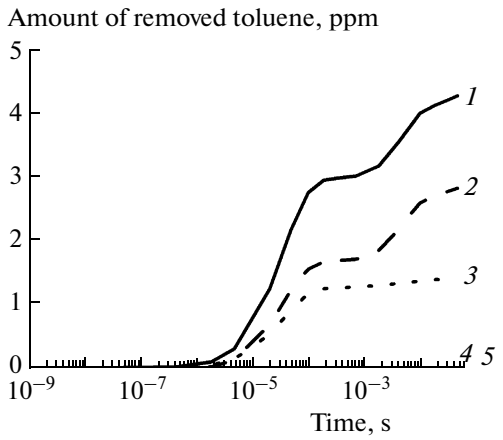

Fig. 9. The same as in Fig. 8, but for $[O_2] = 10\%$: (*1*) total $C_6H_5CH_3$ removal; (*2*) reaction (48); (*3*) reaction (27); (*4*) reactions (10), (12), and (13); and (*5*) reaction (11).

postdischarge stage of the second current pulse in the mixture $N_2 : O_2$ at the optimum oxygen concentration $[O_2] = 0.1\%$. Similar dependences for the last, 100th, current pulse are shown in Fig. 7.

It is easily seen from the results shown in Figs. 6 and 7, in the case of the multipulse effect of the discharge on the polluted gas flow, the amount of removed toluene in each current pulse monotonically decreases with the pulse number. An analysis of the results presented in Figs. 6a–6c and 7a–7c shows that the main specific mechanisms of $C_6H_5CH_3$ decomposition correspond to each time interval in the postdischarge stage. For short times after the discharge end, the main channels of toluene decomposition are controlled by its reactions (10)–(13) with metastable nitrogen molecules. For later times, the main channel of $C_6H_5CH_3$ decomposition changes, i.e., the hydroxyl radical OH generated in plasma-chemical reactions becomes a main reagent with toluene due to reaction (48). It is interesting to note that atomic oxygen O also appreciably contributes to $C_6H_5CH_3$ removal at this stage (reaction (27)); however, the amount of removed toluene due to channel (27) is about two times smaller than in reaction (48). A comparison of Figs. 6 and 7 shows that the duration of the stage of plasma-chemical toluene conversion in the postdischarge phase due to reactions (27) and (48) between $C_6H_5CH_3$ molecules and radicals OH and O becomes shorter with the current pulse number, whereas the duration of reactions (10)–(13) increases. This is due to gradual generation of plasma-chemical toluene decomposition products in the treated gas mixture, which actively interact with radicals OH and atoms O. These processes increase the $C_6H_5CH_3$ treatment (oxidation) depth; however, they appreciably lower the contribution of channels (27, 48) to primary toluene decomposition. It is interesting to note that the absolute amount of toluene removed due to its reactions with $N_2(A^3\Sigma_u^+)$ and $N_2(a'^1\Sigma_u^-)$ molecules remains almost unchanged over the entire toluene removal process. An analysis of Figs. 6 and 7 shows that the main contribution to toluene removal during the first current pulses (Fig. 6e) at the optimum oxygen concentration is made by the hydroxyl radical OH and oxygen atoms O (60 and 20%, respectively). The contribution of metastable nitrogen molecules is ~17%. At the same time, as the simulation results in Fig. 7e show, the contribution of $N_2(A^3\Sigma_u^+)$ and $N_2(a'^1\Sigma_u^-)$ molecules to $C_6H_5CH_3$ decomposition during the last current pulses is more than 50%.

Figures 8 and 9 show the numerical simulation results presenting the contribution of the main channels of toluene decomposition during the second current pulse at oxygen concentrations $[O_2] = 1.5\%$ (8) and $[O_2] = 10\%$ (9). We can see that the main channel of toluene removal at these oxygen concentrations is associated with the hydroxyl radical OH (reaction (48)). A comparison of Figs. 6d, 8, and 9 shows that the contribution of this channel to total $C_6H_5CH_3$ removal increases with $[O_2]$. We note that the contribution of each current pulse to toluene removal monotonically decreases as its number increases at the optimum oxygen concentration $[O_2] = 0.1\%$; however, the difference between the first and last (100th) pulses significantly decreases with the oxygen concentration in the gas mixture. This is caused by a decrease in the contribution of metastable nitrogen molecules to $C_6H_5CH_3$ decomposition with the oxygen concentra-

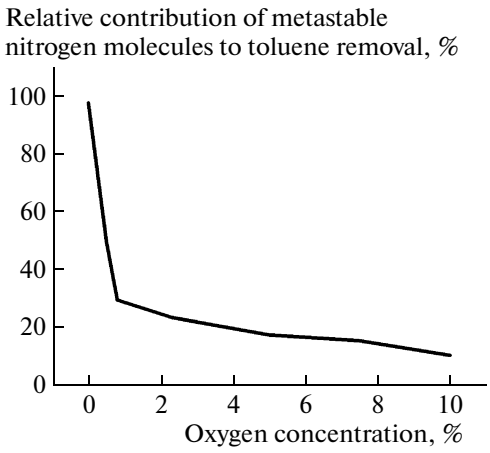

Fig. 10. Relative contribution of metastable $N_2(A^3\Sigma_u^+)$ and $N_2(a'\Sigma_u^-)$ nitrogen molecules to the total toluene removal as a function of the oxygen concentration at the initial toluene concentration $[C_6H_5CH_3]_0 = 400$ ppm and gas temperature $T = 323$ K.

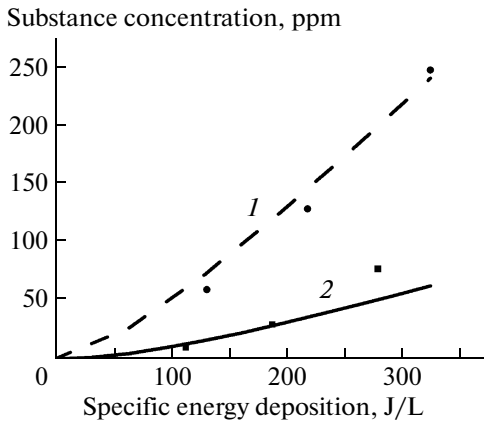

Fig. 11. Dependence of the (*1*) carbon monoxide CO and (*2*) carbon dioxide CO_2 concentration at the plasma-chemical reactor output on the specific energy deposition in the gas mixture $N_2 : O_2$ at the initial toluene concentration $[C_6H_5CH_3]_0 = 400$ ppm, oxygen concentration $[O_2] = 1.5\%$, and gas temperature $T = 323$ K. The curves show the simulation results, and the symbols show the experimental data [9].

tions $[O_2]$. The calculated results show that the basic decrease in the degree of toluene removal with increasing $[O_2]$ occurs exactly during the first current pulses; whereas the amount of decomposed toluene during the last pulses is almost independent of the oxygen concentration.

Figure 10 show the data on the relative contribution of reactions (10)–(13) to the total toluene removal as a function of the oxygen concentration in the gas mixture. We note that these data reflect only direct $C_6H_5CH_3$ decomposition by metastable N_2 molecules due to reactions (10)–(13) and ignore their contribution to generation of atoms O and radicals OH due to generation of H and O atoms in reactions (10)–(13), as well as in reactions (8) and (96),

$$N_2\left(A^3\Sigma_u^+\right) + O_2 \rightarrow O + O + N_2, \quad (8)$$

$$N_2\left(a'^1\Sigma_u^-\right) + O_2 \rightarrow O + O + N_2. \quad (96)$$

We can see that the contribution of metastable $N_2(A^3\Sigma_u^+)$ and $N_2(a'^1\Sigma_u^-)$ molecules to toluene decomposition decreases as $[O_2]$ increases; however, it remains appreciable to $[O_2] = 5\%$.

An analysis of the main channels of toluene decomposition at various oxygen concentrations, performed within the developed model, allowed understanding of the cause of the existence of the optimum O_2 concentration during $C_6H_5CH_3$ removal. First, we note that the role of metastable N_2 molecules in the toluene removal mechanism due to reactions (10)–(13) decreases (Fig. 10) with increasing $[O_2]$, since these molecules are efficiently quenched by molecular oxygen in reactions (8) and (96). As simulation showed, the number of O atoms generated in the discharge significantly increases to the concentration $[O_2] = 0.1\%$ as the molecular oxygen concentration in the gas mixture increases. When the oxygen concentration in the mixture exceeds 0.1%, the density of O atoms in the discharge is significantly slowed down; in this case, the rate of O atom conversion to ozone increases (reactions (80), (81)), which, as is known, is not involved in the toluene decomposition mechanism. Thus, there simultaneously exist competing channels of O atom expenditure: decomposition of toluene and other products of its decomposition, generation of hydroxyl radicals OH in reaction (18) (which also destructs $C_6H_5CH_3$), and ozone formation. The importance and relative contribution of these processes vary with oxygen and toluene concentrations in the gas mixture. A comparative analysis of numerical simulation results on ozone generation in the gas mixture $N_2 : O_2$ in the presence of toluene and in its absence showed that appreciable ozone generation (at the level of ≥30 ppm) begins only at $[O_2] > 0.1\%$ at the toluene concentration $[C_6H_5CH_3]_0 = 400$ ppm in the mixture. Thus, the existence of the optimum concentration $[O_2]$ in the toluene removal mechanism is associated with ozone formation processes.

The presence of molecular oxygen O_2 in the gas mixture $N_2 : O_2$ has a significant effect on the composition of intermediate and final products of plasma-chemical toluene conversion. First of all, it should be noted that an oxygen additive results in total disappearance of such an ecologically hazardous final product of toluene decomposition in nitrogen as cyanic hydrogen HCN.

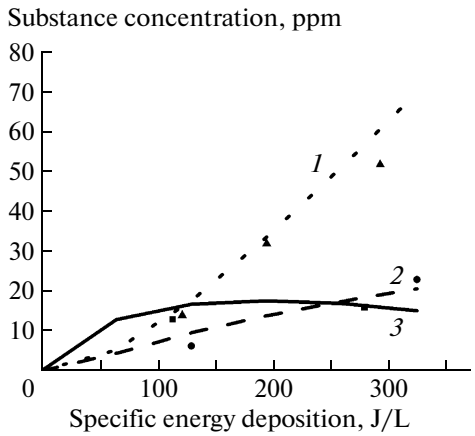

Fig. 12. Dependence of the concentrations of (*1*) formic acid HCOOH (triangles and dotted curve), (*2*) formaldehyde CH_2O (circles and dashed curve), and (*3*) benzaldehyde C_6H_5CHO (squares and solid curve) at the plasma-chemical reactor output on the specific energy deposition in the gas mixture $N_2 : O_2$ at the initial toluene concentration $[C_6H_5CH_3]_0 = 400$ ppm, oxygen concentration $[O_2] = 1.5\%$, and gas temperature $T = 323$ K. The curves show the simulation results, and the symbols show the experimental data [9].

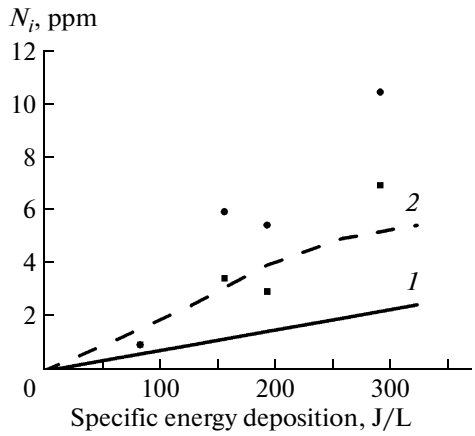

Fig. 13. Dependence of the concentrations of (*1*) CH_3ONO_2 vapor (squares and solid curve) and (*2*) nitric acid HNO_3 (circles and dashed curve) at the plasma-chemical reactor output on the specific energy deposition in the gas mixture $N_2 : O_2$ at the initial toluene concentration $[C_6H_5CH_3]_0 = 400$ ppm, oxygen concentration $[O_2] = 10\%$, and gas temperature $T = 323$ K. The curves show the simulation results, and the symbols show the experimental data [9].

Figures 11–13 show the generation kinetic curves for some by-products detected in the experiment [9].

In the experiment [9], the concentration of carbon oxides at high specific energy depositions ($Q > 150$ J/L at temperature $T = 323$ K) monotonically increased with the discharge glow time, reaching a steady state in ~6 min of discharge operation. Two possible explanations of the observed effect are proposed in [9]: (i) a gradual increase in the discharge zone temperature followed by its stabilization due to thermal conductivity, which leads to a change in the oxidation rate of intermediate products, and (ii) oxidation of deposits on gas-discharge chamber walls. None of these supposed processes was considered in the numerical simulation. Therefore, the numerical simulation results on carbon oxide generation (Fig. 11) were compared with experimental data obtained immediately after turning-on the discharge.

The presented numerical simulation results show that the developed kinetic model adequately predicts the formation of a large number of experimentally observed intermediate and final products of plasma-chemical toluene decomposition. An estimation of the degree of selectivity of $C_6H_5CH_3$ decomposition to final stable products CO and CO_2 shows that up to ~22% of decomposed toluene transform to these products at the specific energy deposition $Q = 325$ J/L; as seen in Fig. 11, the CO concentration is noticeably higher than the CO_2 concentration.

4. CONCLUSIONS

(i) The kinetic model of plasma-chemical toluene decomposition in nonequilibrium low-temperature plasma in pure nitrogen and the mixture $N_2 : O_2$ was developed. The results of numerical calculations using the developed model are in qualitative and quantitative agreement with available experimental data on both the efficiency of plasma-chemical toluene removal and the composition and concentration of intermediate and final products of $C_6H_5CH_3$ conversion.

(ii) The main channels of toluene decomposition in nonequilibrium low-temperature nitrogen plasma are associated with metastable $N_2(A^3\Sigma_u^+)$ and $N_2(a'^1\Sigma_u^-)$ nitrogen molecules.

(iii) The presence of oxygen in the initial gas mixture significantly changes the toluene decomposition kinetics and significantly increases its removal efficiency in comparison with the discharge in pure nitrogen.

(iv) There is an optimum molecular oxygen concentration in the mixture $N_2 : O_2$, at which the maximum efficiency of toluene removal is achieved. The optimum O_2 concentration increases with the initial toluene concentration.

(v) In the gas mixture $N_2 : O_2$, the largest contribution to $C_6H_5CH_3$ decomposition is made by the toluene reaction with the hydroxyl radical OH, which in turn is generated due to plasmachemical reactions between $C_6H_5CH_3$ decomposition products and oxygen atoms.

(vi) The presence of oxygen in the initial gas mixture changes significantly, in comparison with pure nitrogen, the composition of intermediate and final products of plasma-chemical decomposition of toluene.

ACKNOWLEDGMENTS

The authors are grateful to N.A. Dyatko, A.P. Napartovich, B.V. Potapkin, S.Ya. Umanskii, and M.A. Deminskii for fruitful discussion of the results of the study. This study was supported by the Russian Foundation for Basic Research, project no. 10-02-01289a.

REFERENCES

1. K. Urashima and J. S. Chang, IEEE Trans. Dielec. Electr. Insul. **7**, 602 (2000).
2. S. Pekarek, V. Kriha, M. Pospesil, and I. Viden, J. Phys. D **34**, L117 (2001).
3. Yu. S. Akishev, V. B. Karalnik, I. V. Kochetov, et al., in *Proceedings of the 16th International Symposium on Plasma Chemistry, Taormina, 2003*, p. 226.
4. R. Vertriest, R. Morent, J. Dewulf, et al., Plasma Sources Sci. Technol. **12**, 412 (2003).
5. S. Ognier, L. Martin, and J. Amouroux, in *Proceedings of the 17th International Symposium on Plasma Chemistry, Toronto, 2005*, p. 604.
6. M. Magureanu, N. Mandache, C. Preda, and V. Parvulescu, in *Proceedings of the 2nd International Workshop on Cold Atmospheric Pressure Plasmas: Sources and Applications, Bruges, 2005*, p. 242.
7. Z. Machala, M. Morvova, E. Marode, and I. Morva, J. Phys. D **33**, 13198 (2000).
8. V. A. Bityurin, E. A. Filimonova, and G. V. Naidis, IEEE Trans. Plasma Sci. **37**, 911 (2009).
9. N. Blin-Simiand, F. Jorand, L. Magne, et al., Plasma Chem. Plasma Process. **28**, 429 (2008).
10. Z. Falkenstein, J. Appl. Phys. **85**, 525 (1999).
11. H. M. Lee and M. B. Chang, Plasma Chem. Plasma Process. **23**, 541 (2003).
12. Z. Machala and K. Hensel, in *Proceedings of the 2nd International Workshop on Cold Atmospheric Pressure Plasmas: Sources and Applications, Bruges, 2005*, p. 97.
13. C. Jiang, A. Mohamed, R. Stark, et al., IEEE Trans. Plasma Sci. **33**, 1416 (2005).
14. K. Urashima, J. S. Chang, and T. Ito, in *Proceedings of the Annual Meeting of the IEEE Industry Applications Society, New Orleans, LA, 1997*, p. 1969.
15. H. H. Kim, A. Ogata, and S. Futamura, J. Phys. D **38**, 1292 (2005).
16. De-Zeng Yang, Wen-Chun Wang, Shou-Zhe Li, et al., J. Phys. D **43**, 455202 (2010).
17. Yu. S. Akishev, M. E. Grushin, I. V. Kochetov, et al., Plasma Phys. Rep. **26**, 157 (2000).
18. R. Brandenburg, V. A. Maiorov, Yu. B. Golubovskii, et al., J. Phys. D **38**, 287 (2005).
19. O. Eichwald, O. Ducasse, D. Dubois, et al., J. Phys. D **41**, 234002 (2008).
20. R. Ono and R. Oda, J. Phys. D **37**, 730 (2004).
21. R. Ono and R. Oda, J. Phys. D **41**, 035204 (2008).
22. V. T. Samoilovich, V. I. Gibalov, and K. V. Kozlov, *Physical Chemistry of Barrier Discharge* (Izd. Mosk. Gos. Univ., Moscow, 1989) [in Russian].
23. I. Kossyi, A. Y. Kostinskii, A. A. Matveev, and V. P. Silakov, Plasma Sources Sci. Technol. **1**, 207 (1992).
24. Yu. S. Akishev, A. A. Deryugin, V. B. Karal'nik, et al., Plasma Phys. Rep. **20**, 511 (1994).
25. A. V. Phelps and L. C. Pitchford, Report No. 26 (Univ. of Colorado, Boulder, CO, 1985).
26. R. J. W. Henry, P. G. Burke, and A. L. Sinfailam, Phys. Rev. **178**, 218 (1969).
27. K. A. Berrington, P. G. Burke, and W. D. Robb, J. Phys. B **8**, 2500 (1975).
28. M. Capitelli, C. M. Ferreira, B. F. Gordiets, and A. I. Osipov, Springer Ser. At. Opt. Plasma Phys. **31** (2000).
29. A. A. Ionin, Yu. M. Klimachev, A. Yu. Kozlov, et al., J. Phys. D **42**, 015201 (2009).
30. M. Yousfi, N. Azzi, P. Segur, et al., *Electron–Molecule Collision Cross Sections, Electron Swarm Parameters in Some Atmospheric Gases (N_2, O_2, CO_2, H_2O)* (Centre de Physique Atomique de Toulouse & Istituto di Elettrotecnica ed Elettronica Università di Padova, Toulouse–Padova, 1987).
31. M. J. McEwan and L. F. Phillips, *Chemistry of the Atmosphere* (Halsted, New York, 1975; Mir, Moscow, 1978).
32. A. H. Chang and S. H. Lin, Chem. Phys. Lett. **384**, 235 (2004).
33. S. Vranckx, J. Peeters, and S. Carl, Phys. Chem. Chem. Phys. **10**, 5714 (2008).
34. D. Smith, N. G. Adams, and E. Alge, Chem. Phys. Lett. **105**, 317 (2002).
35. K. S. Klopovsky, A. V. Mukhovatova, A. M. Popov, et al., J. Phys. D **27**, 1399 (1994).
36. S. Williams, S. Arnold, A. Viggiano, et al., in *Proceedings of the 52nd Annual Gaseous Electronics Conference, Norfolk, VA, 1999*, p. 10.
37. E. Marotta, A. Callea, X. Ren, et al., Plasma Process. Polym. **5**, 146 (2008).
38. L. V. Gurvich, G. V. Karachentsev, V. N. Kondrat'ev, et al., *Energy of Chemical Bond Cleavage. Ionization Potentials and Electron Affinity* (Nauka, Moscow, 1974) [in Russian].
39. O. V. Mazurin, *Electrical Properties of Glass* (Lengoskhimizdat, Leningrad, 1962) [in Russian].
40. D. Braun, V. Gibalov, and G. Pietsch, Plasma Sources Sci. Technol. **1**, 166 (1992).
41. B. Eliasson and U. J. Kogelschatz, J. Phys. B **19**, 1241 (1986).
42. B. Eliasson and U. J. Kogelschatz, IEEE Trans. Plasma Sci. **19**, 309 (1991).
43. V. Wagner, M. E. Jenkin, S. V. Saunders, et al., Atmos. Chem. Phys. **3**, 89 (2003).
44. E. G. Alvarez, J. Viidanoja, and A. Muniz, Environ. Sci. Technol. **41**, 8362 (2007).

45. J. A. Manion, R. E. Huie, R. D. Levin, et al., *Chemical Kinetics Database, NIST Standard Reference Database 17. Ver. 7.0, Release 1.6.4. Data version 2011.11* (National Inst. of Standards, Technology, Gaithersburg, MD, 2011); http://kinetics.nist.gov/
46. D. I. Slovetskii, *Mechanisms of Chemical Reactions in Nonequilibrium Plasmas* (Nauka, Moscow, 1980) [in Russian].
47. J. T. Herron, J. Phys. Chem. Ref. Data **28**, 1453 (1999).
48. http://www1.chem.leeds.ac.uk//Atmospheric/MCM/mcmproj.html
49. X. Zhong and J. W. Bozzelli, J. Phys. Chem. A **102**, 3537 (1998).
50. J. A. Miller and C. F. Melius, Combust. Flame **91**, 21 (1992).
51. J. Warnatz, H. Bockhorn, A. Mozer, and H. W. Wenz, in *Proceedings of the 19th International Symposium on Combustion, Haifa, 1982*, p. 197.
52. T. Ko, G. Ya. Adusei, and A. Fontijn, J. Phys. Chem. **95**, 8745 (1991).
53. H. -Y. Zhang and J. T. McKinnon, Combust. Sci. Tech. **107**, 261 (1995).
54. M. U. Alzueta, P. Glarborg, and K. Dam-Johansen, Int. J. Chem. Kin. **32**, 32 (2000).
55. M. U. Alzueta, R. Bilbao, A. Millera, et al., Energy Fuels **12**, 1001 (1998).
56. P. Frank, J. Herzler, Th. Just, and C. Wahl, Symp. (Intern.) Combust. **25**, 833 (1994).
57. T. Tanzawa and W. C. Gardiner, J. Phys. Chem. **84** (1980).
58. R. Knystautas, J. H. S. Lee, J. E. Shepherd, and A. Teodorczyk, Combust. Flame **115**, 424 (1998).
59. J. L. Emdee, K. Brezinsky, and I. Glassman, J. Phys. Chem. **96**, 2151 (1992).
60. W. J. Pitz and C. K. Westbrook, Combust. Flame **63**, 113 (1986).
61. J. Meyer, D. Klosterboer, and D. Setser, J. Chem. Phys. **55**, 2084 (1971).
62. S. Suzuki, T. Suzuki, and H. Itoh, in *Proceedings of the XXVIII International Conference on Phenomena in Ionized Gases, Prague, 2007*, p. 220.
63. http://www.kintech.ru/
64. Z. Falkenstein and J. J. Coogan, J. Phys. D **30**, 817 (1997).

Translated by A.M. Kazantsev